The formation process and environment of glendonite and glendonite concretion

（玄能石および玄能石コンクリーションの形成過程と形成環境）

MURAMIYA, Yusuke

（村宮　悠介）

A dissertation for the degree of Doctor of Science

Department of Earth and Environmental Sciences,

Graduate School of Environmental Studies, Nagoya University

（名古屋大学大学院環境学研究科地球環境科学専攻学位論文　博士（理学））

2022

Contents:

Abstract

Glendonite is generally accepted as a pseudomorph after ikaite ($CaCO_3 \cdot 6H_2O$) and is commonly preserved in spherical carbonate concretions known as glendonite concretions in marine sedimentary rocks. Glendonites and glendonite concretions has long been used as an indicator of low-temperature environments. Although they have widely attracted attention as environmental indicators, the detailed geochemical process underlying glendonite formation is not fully understood. This study shows the formation process of glendonites and glendonite concretions by compiling information on glendonites and conducting detailed macro- and microscopic observations, carbon and oxygen isotopic ($\delta^{13}C$ and $\delta^{18}O$) analyses, chemical composition analyses, and elemental mapping of glendonite concretions. Geological investigation and sample collection were conducted on four Cenozoic marine sedimentary strata distributed in Japan: middle to late Eocene Poronai Formation, Mikasa, Hokkaido; late Miocene Morai Formation, Ishikari, Hokkaido; early Oligocene Asagai Formation, Iwaki, Fukushima Pref.; and early Miocene Toyohama Formation, Minamichita, Aichi Pref.

Glendonites were found in at least 36 Cenozoic formations in Japan, and glendonite concretions have been found in 19 of these formations. Within the glendonite distribution in Japan, the glendonite concretion distribution is not restricted to a particular region or geological age. This suggests that the formation of glendonite concretion is not an unusual case to a particular region or geological age. The occurrence of glendonites and concretions around dead organisms, such as bivalves, ghost shrimp, or soft-bodied organisms forming ichnofossils, and negative $\delta^{13}C$ values of glendonites and surrounding concretions from −20‰ to −10‰ show that glendonite concretions were formed using carbon derived from dead organisms. Highly concentrated phosphate in glendonites and

surrounding concretions of 2–16 times more than in surrounding matrixes support this interpretation. The phosphorus distribution pattern in glendonite concretions indicates that changes in phosphate concentrations during the decomposition of dead organisms controlled the timing of ikaite growth termination and the beginning of concretion formation. Bending laminae around concretions, undeformed ichnofossils in glendonite concretions, Ca distributions in concretions interpreted by the reaction-front concretion formation model, and $\delta^{18}O$ values of concretions also show that the concretion formation around ikaite crystals was completed in a shallow part of sediments within months to years. This work provides a new phosphate concentration-controlled growth model of glendonite concretions involving organic decomposition to evaluate the chemical conditions of porewater during early diagenesis.

Chapter 1. Background

1-1. Introduction

Spherical carbonate concretions are dense and hard spherical-shaped carbonate aggregations observed in sedimentary rocks globally (Marshall and Pirrie, 2013). Concretions typically contain well-preserved fossils inside (Baird et al., 1986; Martill, 1988; Maeda and Shigeta, 2005; Landman and Klofak, 2012; Plet et al., 2017; Clements et al., 2019; Jauvion et al., 2020). Therefore, fossils in the concretions and information on geochemical conditions during the concretion formation have long attracted many earth scientists.

Calcium carbonate concretions form rapidly due to the reaction with calcium ions in seawater and bicarbonate from dead organisms in the center of concretions during the early diagenesis (Yoshida et al., 2015, 2018, 2020). Such rapid concretion formations cause the consolidation around fossils before their deformation due to sediment compaction and preserve delicate three-dimensional fossil morphology (e.g., Martill, 1988; Maeda and Shigeta, 2005; Jauvion et al., 2020). Moreover, concretions sometimes preserve highly labile soft tissues and soft-bodied organisms (Baird et al., 1986; Martill, 1988; Clements et al., 2019; Jauvion et al., 2020). Some concretions containing well-preserved fossils are known as famous fossil Lagerstätten, such as the concretions from the Mazon Creek, Illinois, USA, and those from Ceará, Brazil, which have provided us with a high opportunity to understand paleoorganisms (Baird et al., 1986; Martill, 1988).

Concretions prevent secondary alteration of fossils and clastics due to carbonate cementation (Muramiya et al., 2020). Miocene Morozaki Group distributed in Japan contains dolomite concretions in tuffaceous sandstone strata. Volcanic glasses observed

in the surrounding matrices of concretions altered and completely transformed to heulandite, whereas those in concretions are unaltered. Volcanic glasses in concretion have been protected from the alteration by cementation of dolomite in concretion, which decreases the permeability of concretion and prevents elemental migration (Muramiya et al., 2020).

Concretions also provide geochemical information on sedimentary environments during concretion formation in early diagenesis. For example, the porewater's redox conditions and chemical compositions during concretion formation were recorded in the forming minerals and chemical compositions (Matsumoto and Iijima, 1981; Curtis et al., 1986; Hendry et al., 2006). Carbon and oxygen isotopic ($\delta^{13}C$ and $\delta^{18}O$) compositions of carbonate minerals in concretions are widely applied as an indicator of the organic decomposition process and temperature when concretions are formed (Irwin et al., 1977; Coleman, 1993; Mozley and Burns, 1993; Dale et al., 2014; Muramiya et al., 2017, 2020). Also, the recent discovery of rapid concretion formation (Yoshida et al., 2015, 2018, 2020) has enabled us to measure the age of concretion-bearing strata from strontium isotopic compositions of concretions (Yoshida et al., 2019).

Although numerous studies on carbonate concretions have been conducted, little is known about the formation process of glendonite concretions, which contain glendonite in the center (Fig. 1). Glendonite is a pseudomorph after ikaite ($CaCO_3 \cdot 6H_2O$) with bipyramidal or stellate crystal shapes (Shearman and Smith, 1985; Frank et al., 2008; Vickers et al., 2018; Rogov et al., 2021), mainly composed of calcite ($CaCO_3$). Glendonite is observed in marine sediments and sedimentary rocks of the Paleozoic to Quaternary ages globally (Teichert and Luppold, 2013; Wang et al., 2017; Popov et al., 2019; Vickers et al., 2020; Mikhailova et al., 2021; Rogov et al., 2021). It often occurs in spherical

calcium carbonate concretions known as glendonite concretions (Boggs Jr, 1972; Morikiyo et al., 2018; Muramiya et al., 2022).

Ikaite crystals in marine sediments have been identified within a few meters of burial depth (Kodina et al., 2003; Lu et al., 2012; Kakuwa et al., 2019; Hiruta and Matsumoto, 2022) under conditions of high phosphate concentrations (Kodina et al., 2003; Zhou et al., 2015) and near-freezing temperatures (Suess et al., 1982; Kodina et al., 2003; Zhou et al., 2015). In the natural environment, ikaite has only been found in environments with water temperatures below 7 °C (Pauly, 1963; Suess et al., 1982, Buchardt et al., 2001; Dieckmann et al., 2010). Under moderately warm temperatures, ikaite crystals instantly release the water from the crystal to transform into an aggregation of granular calcite (Suess et al., 1982; Jansen et al., 1987). Because of this temperature sensitivity of ikaite stabilization, glendonites and glendonite concretions have been widely used as indicators of cold temperature to reconstruct paleoenvironments (De Lurio and Frakes, 1999; Grasby et al., 2017; Jones et al., 2006; Price, 1999; Rogov et al., 2017; Rogov and Zakharov, 2010; Spielhagen and Tripati, 2009; Vickers et al., 2020). Even though many scientists have focused on paleoenvironmental indicators, the detailed glendonite and glendonite concretion formation processes are not fully understood, and the following questions remain.

First, what are the carbon sources of ikaite and its surrounding concretions? The supply and accumulation of a substantial amount of carbon are necessary to form ikaite crystals and surrounding calcite concretions. Although previous studies have proposed the contributions of bacterial organic decomposition and methane in the sediments to glendonite concretion formation based on the $\delta^{13}C$ and the biomarkers preserved within them (Teichert and Luppold, 2013; Qu et al., 2017; Morikiyo et al., 2018), the concrete

carbon source is still unclear.

Second, why is glendonite in the center part of glendonite concretions? Most glendonite concretions observed globally contain glendonites observed in the center part. This morphology indicates that the formation of glendonite concretion first requires the ikaite crystal formation, then the subsequent calcite concretion formation around glendonite (or preceding ikaite crystal). However, what factor controls such a sequential process during glendonite concretion formation is unknown.

Third, why is there a variation in the relative size of concretions compared to glendonites within a stratum? Some glendonites are completely enveloped by concretions; however, termination of other glendonites in concretions thrust out concretion surfaces. Moreover, some glendonites are not contained in concretions but are directly buried in the host rock. Although such variation can be observed globally (Boggs Jr, 1972; Teichert and Luppord, 2031; Vasileva et al., 2021), the reason is little explained.

This thesis addresses the above questions by showing the sequential formation process of glendonites and glendonite concretions based on detailed geological observations and geochemical analyses from several Cenozoic marine strata in Japan. This study's results revealed that dead organisms supplied carbon to form both ikaite and the surrounding concretions and changes in the porewater's phosphate concentrations switched the ikaite precipitation to the surrounding calcite concretion formation. This phosphate-controlled formation model explains the variations in the relative sizes of concretions compared to glendonites. The glendonite concretion formation process identified in this study indicates that the modes of glendonite occurrence can be applied globally as an indicator of the geochemical conditions in early diagenesis.

1-2. Geological setting

This study investigated four successions of Cenozoic glendonite concretion-bearing marine strata distributed in Japan: 1) Eocene Poronai Formation and 2) Miocene Morai Formation in Hokkaido, northern Japan; 3) Oligocene Asagai Formation in Fukushima, northeastern Japan; 4) Miocene Toyohama Formation in Aichi, central Japan (Figs. 2 and 3).

The Poronai Formation is distributed in the central part of Hokkaido, Japan, and outcrops along the Ikushumbetsu and Mikasa–Horonai rivers in the Mikasa area. The Poronai Formation comprises massive dark-gray mudstone with minor interbedded fine sandstone, is more than 1600-m thick (Matsuno et al., 1964), and is divided into lower and upper parts based on facies and fossil fauna. The lower part comprises unbedded dark-gray mudstone, except the lowermost part containing conglomerate, fine sandstone, and sandy siltstone. The upper part consists of bedded sandy siltstone. Foraminifera assemblages show that the Poronai Formation was deposited in the middle to late Eocene (Okada and Kaiho, 1992). The Poronai Formation yields abundant fossils of marine organisms, such as bivalves, gastropods, crustaceans, and cephalopods. Molluscan assemblages indicate that the Poronai Formation's lower part, which frequently contains glendonite concretions, was deposited on the lower sublittoral to the upper bathyal seabed (Suzuki, 2000). Glendonite with and without concretions are observed in bioturbated muddy facies. They are both abundantly found form several horizons, but they do not occur together from the same horizon. Their horizontal distributions are uncertain because it is difficult to trace a stratum horizontally due to unbedded facies. Spherical concretions without glendonites are also abundantly found in bioturbated muddy facies and typically contain fossils of articulated bivalves or crustaceans.

The Morai Formation is distributed in the central part of Hokkaido and primarily consists of weakly bedded silicic mudstone, and it outcrops along the Japan Sea coast of the Ishikari area. Diatom assemblages in the Morai Formation show a late Miocene depositional age (The Kabato Collaborative Research Group, 1995). The Morai Formation contains abundant fossils of marine organisms, including bivalves, gastropods, scaphopods, crustaceans, and echinoids. The sedimentary facies and fossil assemblage indicate that the Morai Formation was deposited in the bathyal zone at a water depth of 200–300 m (Takano et al., 1996; Tsushima et al., 1956). Glendonite concretions are observed in one horizon of bioturbated muddy facies. Judging from the distribution of glendonite concretions falls from the outcrop, their horizontal distribution extends for at least 300 m. Spherical concretions without glendonites are found in several horizons of bioturbated muddy facies, and most contain articulated bivalves, gastropods, scaphopods, or aggregation of ichnofossils.

The Asagai Formation outcropped at Iwaki and distributed in the southern part of Fukushima primarily comprises massive, blue-gray and dark-gray, fine to very-fine sandstone (Suto et al., 2005). Fossil assemblages of mollusks, Dinophyceae, and benthic foraminifera indicate that the Asagai Formation was deposited during the early Oligocene (Suto et al., 2005). The Sr isotopic dating using the shell fossils shows ages of 37.8 Ma and 37.9 Ma (Ogasawara et al., 2001), and the sedimentary facies indicate that the Asagai Formation was deposited at the upper to lower shoreface and the inner shelf (Ueda et al., 2003). Glendonite concretions, glendonites without concretions, and spherical concretions without glendonites formed in the bioturbated massive gray siltstone, and each is observed in different horizons. The horizontal distribution of the glendonite-bearing horizon is uncertain because of poor and limited exposure of the outcrop.

The Toyohama Formation in southern Aichi consists of alternating beds of tuffaceous sandstone and mudstone (Muramiya et al., 2020) and outcrops along the coast of the Minamichita area. The Toyohama Formation contains abundant fossils of bivalves, gastropods, crustaceans, and echinoids (Muramiya et al., 2020). Diatom assemblages indicate that the Toyohama Formation was deposited during the early Miocene (Ito et al., 1999), and molluscan fossil assemblages suggest that the Toyohama Formation was deposited on the seafloor at a depth of 100–300 m (Shikama and Kase, 1976). Glendonite concretions and spherical concretions without glendonites are observed in bioturbated tuffaceous mudstone, and the distribution of the layer with glendonite concretions extends horizontally to at least 100 m.

Chapter 2: Methods

2-1. Literature review

The frequency of glendonite without concretion and glendonite concretion and depositional environments of glendonite-bearing strata in Japan were evaluated by searching glendonite records in the literature, including journal articles, university bulletins, scientific books, and explanation papers with geological maps. Records of their occurrence are compiled for each formation. For the glendonite-bearing strata, their distributions, ages, lithofacies, and paleowater depth are also collected.

2-2. Field observations and sampling

Field observations and sampling for laboratory observations and analyses were

conducted for the four formations: the Poronai Formation, which outcrops along the Ikushumbetsu and Mikasa–Horonai rivers in the Mikasa area, Hokkaido, Japan; the Morai Formation, which distributes along the Japan Sea coast of the Ishikari area, Hokkaido, Japan; The Asagai Formation, which is artificially exposed because of the construction of a wood storage yard at Iwaki, Fukushima Prefecture, Japan; and the Toyohama Formation, which outcrops on the Ise Bay of the Pacific in Minamichita area, Aichi Prefecture, Japan.

Glendonite concretions, glendonites without concretions, spherical concretions without glendonites, shell fossils, and the surrounding matrix were collected from each formation. Glendonites with and without concretions were collected with the matrix. Fragile samples were reinforced using instant glue that did not affect geochemical analyses. Samples were selected from the outcrops' freshest parts by removing weathered surface rocks to reduce the effects of weathering; however, samples from the Asagai Formation might have suffered a meteoric alteration of $\delta^{18}O$ because of relatively prolonged exposure to the outcrops.

2-3. Laboratory observations

The detailed structures in and around the glendonite with and without concretions were observed using cross-section and thin-section samples. Samples were reinforced using resin and cut perpendicular or parallel to the glendonite's long axis. Cut samples were polished with a fine abrasive compound, and some polished samples were left outside to allow slight natural weathering for approximately two weeks with occasional rains, to enhance visual observation of the surface. Samples were observed using stereoscopic and polarizing microscopes.

2-4. Dissolution experiment

Concretions around glendonites from the Poronai Formation were dissolved using buffered acetic acid to obtain microfossils in concretions. The buffer solution for the experiment was prepared using Koot's (2003) method. Concretions around glendonites were cut with a microcutter to produce cubic samples of approximately 1 cm^2, and 26 samples from 15 concretions were dissolved. After dissolving overnight, the residue was collected with a paper filter. This process was repeated three times to dissolve approximately half of the sample volume.

2-5. Mineral composition

Samples were collected from the fresh parts of the cut samples using a microdrill and microcutter, and the samples were powdered using an agate mortar. The powdered samples were analyzed using X-ray diffraction (XRD) to determine mineral compositions. Analyses were conducted with Cu-Kα radiation (operating voltage/current 40 kV/40 mA) at a scan rate of $4°min^{-1}$ using an X-ray diffractometer (MultiFlex, Rigaku) from the Nagoya University Museum, Japan. Bulk glendonites, concretions, surrounding matrixes, and bivalve shell fossils were analyzed.

2-6. Chemical composition and elemental distribution

The major elements (SiO_2, TiO_2, Al_2O_3, Fe_2O_3, MnO, MgO, CaO, Na_2O, K_2O, and P_2O_5) were measured using X-ray fluorescence (XRF) spectroscopy. The bulk glendonite, concretion, and matrix samples collected with a microdrill or microcutter were powdered using an agate mortar. The powdered samples were heated at 500 °C for 2 h and subsequently at 1000 °C for 3 h to remove volatile components such as water in clay

minerals and carbon dioxide in carbonate minerals. The ignited glendonite samples, primarily comprising CaO, were diluted with a pure SiO_2 reagent to input the results within the range of the calibration curve. The ignited samples were powdered again with an agate mortar and mixed with precisely 10 times the sample weight of $Li_2B_4O_7$ and two drops of an aqueous solution LiI. The procedure from heating to mixing with reagents was conducted as quickly as possible to minimize water adsorption on the samples.

The mixtures were fused to make glass beads That were analyzed using an XRF spectrometer (ZSX Primus II, Rigaku) housed at the Graduate School of Environmental Studies, Nagoya University, Japan. The calibration curves for measurements were made using the rock reference material JLs-1 (limestone obtained from Hokkaido, Japan), JB-1a (basalt obtained from Nagasaki, Japan), and JR-2 (rhyolite obtained from Nagano, Japan) provided by the Geological Survey of Japan. The estimated analytical uncertainties were 1%–2% for SiO_2 and Al_2O_3 and 5% for other elements. The loss on ignition (LOI), which corresponds to the weight of volatile components such as water and carbon dioxide, was calculated from the difference in weight between the original and ignited samples, expressed using Equation (1) as

$$LOI = \frac{(W_0 - W_i)}{W_0} \times 100, \quad (1)$$

where W_o (g) is the weight of the original sample, and W_i (g) is the weight of the ignited sample.

Elemental composition and distribution analyses of glendonites in 400 μm × 300 μm were conducted using an electron probe microanalyzer (EPMA) on polished thin-sections covered with a 30-nm-thick carbon coating before analyses. Analyses were performed

using JXA-8200 of JEOL Ltd. housed at the Center for Advanced Marine Core Research, Kochi University, Japan, under the following conditions: a 15-kV acceleration voltage, a 20-nA current beam, and 1-μm beamwidth. The measured elements for point analyses were Si, Al, Fe, Mn, Mg, Ca, K, P, and S. Analytical standards are well-characterized natural minerals and synthetic substances provided by JEOL Ltd. (SiO_2, Al_2O_3, Fe_2O_3, MnO, MgO, $CaSiO_3$, $KalSi_3O_8$, $KTiOPO_4$, and $BaSO_4$). The analyzing crystals were thallium acid phthalate for Si Kα, Al Kα, and Mg Kα, LIFH for Fe Kα, lithium fluoride for Mn Kα, pentaerythritol for Ca Kα and K Kα, and PETH for P Kα and S Kα. The measurement errors were estimated to be less than ±3%, and the detection limits were less than 100 ppm. Elemental distribution maps were generated for Fe, Mn, Mg, Ca, P, and S.

The 2D semiquantitative elemental distribution on the surface of cut and polished samples of glendonite concretions and glendonite without concretion was obtained using a scanning X-ray analytical microscope (SXAM, XGT-5200S of HORIBA Ltd.) at Nagoya University Museum. A high-intensity continuous X-ray beam (Rh anode 50 kV, 1 mA), 100 μm in diameter, was focused using a guide tube and irradiated the sample's surface perpendicularly. XRF from the sample surface was analyzed using a hp-Si detector of an energy-dispersion spectrometer (Katsuta et al., 2003). Elemental distribution maps were generated for Si, Ti, Al, Fe, Mn, Ca, K, S, and Sr.

2-7. Isotopic composition

$\delta^{13}C$ and $\delta^{18}O$ of ikaite-derived granular calcite (Cal-1) in glendonites in concretions, bulk glendonites, concretions, and shell fossils were measured on an IsoPrime isotope ratio mass-spectrometer with an automated MultiPrep carbonate reaction system at the

Center for Advanced Marine Core Research, Kochi University, Japan. The carbonates in matrixes were measured on a stable isotope ratio mass-spectrometer (DELTA V Plus, Thermo Fisher Scientific) equipped with a gas bench, available at Shoko Science Co., Ltd. Japan. Cal-1 samples of glendonite in concretions were carefully separated from the polished samples by scraping them with a steel needle under a microscope. Concretions and bulk glendonite samples were collected from the cut samples using a microdrill. For the bulk glendonites, enough samples (~1 g) were collected to avoid glendonite heterogeneity. For the Asagai Formation, concretions and glendonite partially formed in bivalves and bivalve shells were analyzed. The $\delta^{18}O$ and $\delta^{13}C$ data are expressed in delta notation relative to the Vienna Pee Dee Belemnite (VPDB) standard, in per mill (Craig, 1957). The measurement errors for $\delta^{18}O$ and $\delta^{13}C$ were less than ±0.1‰ for both spectrometers.

Chapter 3: Results

3-1. Distributions of glendonites and glendonite concretions in Japan

Figure 4 shows the localities of glendonite observed in Japan, and Table 1 summarizes the distributions, ages, lithofacies, and paleowater depth of glendonite-bearing strata, including data from field investigations and the literature. Although previous studies indicate that their distribution is limited to the east of the Itoigawa–Shizuoka Tectonic Line (Shibuya, 1977), the results showed that at least 36 formations in Japan contain glendonites, and their distributions extend from Hokkaido to the Aichi Pref. The ages of the glendonite-bearing strata range from Eocene to Pleistocene. Within these

strata, massive fine sandstone to mudstone and alternating beds of sandstone and mudstone are dominant, and in the latter case, most glendonites are contained in mudstone (Fig. 3). All formations are deposited in marine environments, except the Soun Formation, which was deposited in an estuary. Based on the fossil fauna and/or sedimentary facies, most strata are estimated to have been deposited at depths greater than 200 m (For details, see the citations in Table 1 of Muramiya and Yoshida, 2020).

Within the glendonite-bearing strata, glendonite concretions are recognized in 19 formations. Hokoseki, a glendonite concretion with a glendonite-shaped cavity formed by the total dissolution of glendonite, has been found in at least two localities in Japan: the Neogene strata in the Mogami district, Yamagata (Nogoshi, 1966; Takahashi, 1967) and the Jurassic strata in the Rikuzen district, Miyagi (Nire, 1934).

3-2. Occurrence

Figure 1 shows two glendonite occurrences: glendonite observed in a spherical calcite concretion and glendonite without surrounding concretion. In most cases, these two types of glendonites are observed in different stratigraphic horizons in the same stratum. Morphologically, a glendonite concretion has an isolated spherical to ellipsoidal shape with a sharp concretion boundary. The boundary between a concretion and surrounding matrix can easily be distinguished from hardness and color differences. Glendonites and the surrounding concretions are harder than matrixes. The concretions are gray to light gray on a fresh surface, whereas the matrix is a darker color.

Laminae observed in the surrounding sedimentary matrix bend around glendonite concretions and glendonite without concretion, and there is no apparent deformation of ichnofossils in concretions around glendonites. Most glendonites in the concretions have

a bipyramidal shape in the central part of a spherical concretion, and a few glendonites have stellate or X shapes formed in the center of the concretion (Fig. 1). In most cases, glendonite terminations are thrust out of a concretion surface, whereas some glendonites are entirely encapsulated in concretions (Fig. 1). Spherical concretions containing fossils without glendonites are also identified; however, most are found at different stratigraphic levels than glendonite concretions or glendonites without concretions in the same formation.

The Asagai Formation yields glendonite concretions formed around an articulated bivalve (*Mya grewingki*) fossil (Fig. 5a). Specifically, the bivalve's ventral side is at the center of the bipyramidal or stellate-shaped glendonite in the central part of the concretion. Glendonite is also formed in the bivalve and fills the inner space near the ventral side. An aggregation of small ichnofossils is observed in the concretions around glendonites. Glendonites without concretions containing articulated *M. grewingki* at the central part are also observed in the Asagai Formation (Fig. 5b). The bivalve's ventral side is at the center of the glendonite. Glendonite concretions observed in the Toyohama Formation are associated with the ghost shrimp fossil (*Callianopsis titaensis*) in its center (Fig. 6e, f). Although glendonite concretions in the Poronai and Morai formations do not contain macroscopic shell fossils, aggregated small ichnofossils (*Chondrites*) are observed in the concretion matrixes (Fig. 6a–d). These ichnofossils in glendonite concretions preserve their circular cross section.

3-3. Petrology

The microscopic structure of glendonites in concretions is similar in all formations studied. Glendonites in concretions comprise three generations of calcite: (1) granular

calcite distributed uniformly throughout in glendonite (Cal-1), (2) radiaxial calcite grown around Cal-1 (Cal-2), and (3) sparry calcite grown in the remaining pores (Cal-3). Cal-1 is brown with a zoned texture and rounded polygonal shape, approximately 100 μm to 500 μm in diameter (Fig. 7a, b). The characteristics of Cal-1 are common in glendonites globally, and Cal-1 is derived from ikaite (Frank et al., 2008; Huggett et al., 2005; Selleck et al., 2007; Teichert and Luppold, 2013). Cal-1 and Cal-2 occupy more than 90% of the glendonite volume in the concretions (Fig. 7a, b). However, most glendonites without concretions comprise Cal-1 without Cal-2. Quartz and/or sparry calcite fill the pores in glendonites without concretions (Fig. 7c, d). The boundary between a glendonite and a concretion or matrix is sharp, even microscopically. The difference between the surface texture of glendonites within and without concretions is that in concretions, the glendonite surface is smooth, whereas glendonite without concretions has a rough surface texture microscopically (Fig. 7a, b, e, f).

XRD analyses show that glendonites and the surrounding concretions from all four formations primarily comprise calcite (Fig. 8), and some glendonites in concretions contain a minor amount of dolomite or quartz. Glendonites without concretions primarily comprise calcite with quartz. Concretions around glendonites from all four formations are mainly composed of calcite with a mirror amount of quartz and feldspar (Fig. 8). However, no carbonate minerals were detected in the surrounding sedimentary matrixes of all four formations (Fig. 9). The matrixes of the Poronai, Morai, and Asagai formations primarily contain quartz and feldspar, and the Toyohama Formation's matrix comprises clinoptilolite, quartz, and feldspar. Bivalve shells from the Poronai and Asagai formations are preserved as aragonite (Fig. 10).

3-4. Dissolution experiment

Within the residue of the dissolution experiment, some globular and needle-shaped microfossils are obtained from concretions around glendonites from the Poronai Formation (Fig. 11). The former could be shells of foraminifera, and the latter spicules of sponge. Abundant small wood fragments are also obtained.

3-5. Chemical composition and elemental distribution

SXAM elemental mapping of glendonite concretions shows that Ca is concentrated in glendonites and concretions. Ca in a concretion distributes near homogeneously and steeply decreases at the concretion's margin to the surrounding matrix—at a "reaction front" (Yoshida et al., 2015; 2018; 2020) (Fig. 12). Si shows inverted distribution to Ca and is contained in glendonite without concretion. Ca is hardly detected in the surrounding sedimentary matrixes around glendonite concretions and glendonite without concretion (Fig. 13).

XRF analyses show that Ca was highly concentrated in glendonites in concretions, glendonites without concretion, and concretions around glendonites ranging from 17.6 to 41.4 wt%, 42.4 to 47.9 wt%, and 42.4 to 47.9 wt%, respectively. Phosphorus (P) was concentrated from 0.2 to 1.6 wt% in glendonites in concretions and 0.2 to 1.2 wt% in concretions, several times higher than the concentrations of the surrounding sedimentary matrixes (Table 2).

Detailed chemical mapping of glendonites in concretions using EPMA revealed that P was concentrated only within Cal-2 as calcium phosphate (Fig. 14, Table 3).

3-6. Isotopic composition

Figure 15 and Table 4 summarize the isotopic composition of glendonites and related samples. The $\delta^{13}C$ values of glendonites in concretions and without concretions are characterized by negative values from −19.4‰ to −8.6‰ and −31.8‰ to −10.0‰, respectively. Although concretions around glendonites have scattered $\delta^{13}C$ values from −18.0‰ to 0.2‰, negative values around −18‰ to −8‰ are dominant. Fossil-bearing concretions also have negative $\delta^{13}C$ values of −30.7‰ to −13.1‰, and Cal-1, which was carefully separated from glendonites in the concretions from the Poronai Formation, has negative $\delta^{13}C$ values of −21.8‰ to −14.9‰. Carbonate microfossils in matrixes and bivalve fossils have $\delta^{13}C$ values from −7.0‰ to 9.9‰, different from the glendonite and concretion values.

Although the $\delta^{18}O$ values of the concretions around glendonites and fossils vary from −14.3‰ to 2.0‰, most are around 0‰. The $\delta^{18}O$ values of glendonites in concretions and glendonites without concretions were −4.9‰ to 2.2‰ and −1.4‰ to 0.4‰, respectively, and Cal-1 of glendonites in concretions has homogeneous $\delta^{18}O$ values from −2.4‰ to −0.0‰. Carbonate in matrixes and bivalve shell fossils has $\delta^{18}O$ values of −8.2‰ to 2.5‰.

Chapter 4: Discussion

4-1. The formation environment of ikaite and occurrence of glendonites

The glendonites identified in Japan occur in fine-grained sedimentary rocks (Fig. 3, Table 1), and most are observed in gray to black mudstone, which is presumably rich in organic matter. This is not only the case in Japan, as most glendonites globally have been

reported from gray to black muddy rocks (e.g. Selleck et al., 2007; Spielhagen and Tripati, 2009; Teichert and Luppold, 2013; Grasby et al., 2017), and no glendonites were observed in coarse sandstone and conglomerate. Ikaite crystals found in recent marine sediments are also in organic-rich, dark-colored muddy sediments (Suess et al., 1982; Stein and Smith, 1986; Jansen et al., 1987; Lu et al., 2012; Kakuwa et al., 2019). Ikaite crystal formation requires a supply of bicarbonate and high phosphate concentrations, preventing the precipitation of calcite and aragonite (Bischoff et al., 1993; Kodina et al., 2003; Zhou et al., 2015) because phosphate adsorb onto crystal surface of these minerals to decrease precipitation rates (Burton, 1993). Most ikaite crystals in recent marine sediments have $\delta^{13}C$ values that indicate organic-derived carbonates (Suess et al., 1982; Jansen et al., 1987; Greinert and Derkachev, 2004) and form in sediments with high phosphate concentrations in porewater (Kodina et al., 2003; Zhou et al., 2015). In the organic-rich dark-colored muddy sediments, the decomposition of organic matter in sediments and soft tissue of dead organisms richly generate bicarbonate and phosphate (Hensen et al., 2006; Jørgensen, 2006), providing a suitable environment for ikaite precipitation. However, the porewater of coarse-grained quartz and feldspar-rich sediments should have lower bicarbonate and phosphate concentrations than that of muddy sediments because of poor organic matter. Therefore, glendonites occur in organic-rich dark muddy sedimentary rocks, generating a suitable environment for ikaite precipitation.

Most glendonite-baring strata in Japan were deposited in a deep-sea environment (Table 1), probably because of the low temperatures at the bottom of the deep sea. However, the occurrence of glendonite from shallow marine deposits, such as the Yuchi (Pleistocene: Sagayama, 2003), Omagari (late Eocene: Editorial Committee of Hokkaido, Part 1 of Regional geology of Japan, 1990), and Momijiyama (early Oligocene: Kaiho,

1984) formations and the estuarine Soun Formation (late Eocene to early Oligocene: Editorial Committee of Hokkaido, Part 1 of Regional geology of Japan, 1990), shows that low-temperature water existed in the shallow marine and estuary during the deposition of these formations.

Glendonite concretions are found in 19 of 36 formations in Japan that contain glendonites (Table 1), and glendonite concretions are observed in seven of eight prefectures where glendonites are found. There is also no bias in the temporal distribution of glendonite concretions within glendonite distributions. Therefore, the formation of glendonite concretion is not a peculiar case to a particular region or geologic age within which glendonites form (Muramiya and Yoshida, 2020).

4-2. The carbon source of glendonite concretion

In the Asagai Formation, glendonite concretions contain articulated bivalve fossils (*Mya grewingki*), of which the ventral sides are in the centers of bipyramidal or stellate-shaped glendonites (Fig. 5a). The glendonites without concretions also contain articulated *M. grewingki*, with the ventral sides in the centers of the glendonites (Fig. 5b). These occurrences indicate that ikaite crystals and their surrounding concretions grew from the bivalve's ventral side. Finding multiple *M. grewingki* in the centers of the glendonite concretions and glendonites accidentally is highly unlikely because of the low frequency of *M. grewingki* in the Asagai Formation.

The occurrence shows that the following formation processes occurred (Muramiya et al., 2022). When the bivalves died and became buried in the sediments, the soft tissue inside the shells remained because their shells were articulated and closed. Glendonites fill most of the space inside the bivalves, showing that sediments hardly intrude the

bivalves and that soft tissue inside the bivalves remains when they are buried. These occurrences indicate that ikaite crystals and the surrounding concretions formed using organic-derived carbon, which seeped from the gap of ventral sides between the bivalve shells. The estimated pH in the shallow part of the marine sediments (pH 7–8, Shao et al., 2016) indicates that most carbons from dead organisms diffused around as bicarbonate (Drever, 1997). In addition to the glendonites with and without concretions in the Asagai Formation, most glendonite concretions observed in the other sedimentary formations in this study show evidence of organisms, such as ghost shrimp fossil (*C. titaensis*) obtained from the Toyohama Formation (Fig. 6e, f) and ichnofossil *Chondrites* obtained from the Poronai and Morai formations (Fig. 6a–d), formed via vermiform organisms such as Polychaeta (Hertweck et al., 2007; Baucon et al., 2020). These occurrences show that dead organisms supplied bicarbonate to form glendonite concretions and glendonite without concretions.

Most samples of bulk glendonites in concretions, ikaite-derived calcite (Cal-1), surrounding concretions, and bulk glendonites without concretions have negative $\delta^{13}C$ values from −20‰ to −10‰ (Fig. 15, Table 4). Recently, Rogov et al. (2021) showed that most Phanerozoic glendonites and their surrounding concretions globally have the same $\delta^{13}C$ value ranges as shown here. Ikaite-derived calcite inherits $\delta^{13}C$ values from ikaite crystals even after its transformation, confirmed by isotopic analyses of ikaite crystals found in marine sediments (Suess et al., 1982). This preservation potential of ikaite $\delta^{13}C$ and the negative $\delta^{13}C$ values of glendonite concretions and glendonites without concretion indicate that carbon in ikaite crystals and their surrounding concretions are organic in origin because $\delta^{13}C$ values of soft bodies of marine organisms range around −20‰ to −15‰ (Nakashima et al., 2007; Kodama et al., 2011; Ito et al., 2015) (Fig. 15,

Table 4).

Although one highly negative value of glendonite without concretions (−31.8‰) indicates a minor contribution of methane, which has highly negative $\delta^{13}C$ values of approximately −60‰ (Whiticar, 1999), most carbons could have been supplied from the dead organisms in the glendonite concretions and glendonites without concretions. Some fossil-bearing concretions from the Poronai and Toyohama formations also have highly negative $\delta^{13}C$ values of approximately −30‰ (Table 4); however, most values of fossil-bearing concretions indicate that the carbon source is from dead organisms.

Glendonites in concretions and the surrounding concretions contain 0.2 wt% to 1.6 wt% P_2O_5, 2–16 times higher than the concentration in the surrounding matrixes (Table 2). It supports our interpretation that dead organisms supplied carbon to form ikaite and concretions because P is a primary biophilic element liberated from organisms as phosphate during decomposition (Krom and Berner, 1981). Living individuals of Bivalvia; Decapoda, which includes ghost shrimp; and Polychaeta, which is probably a host organism of the ichnofossil *Chondrites*, contain 0.3–1.4 wt% phosphorus in their dried bodies (Brey et al., 2010). The phosphorus concentration in organisms is much higher than in the surrounding matrixes of the glendonite concretions (approximately 0.05 wt%: calculated from XRF data shown in Table 2) and in seawater [1.6×10^{-8} wt%: calculated from the data shown in Nozaki (2001)]. Yoshida et al. (2015, 2018) showed the P concentrations in spherical concretions formed around tusk shells and crustaceans, indicating that dead organisms supplied bicarbonate for ikaite and concretions.

The carbon amount to form ikaite crystal and surrounding concretion has been estimated to assess the contribution of other carbon sources than dead organisms to the formation of glendonite concretion. When it is assumed that all CaO in the sample is

derived from calcite, the carbon content in the sample can be calculated using Equation (2)

$$C_{\text{sample}} = \frac{3}{1400} x_{\text{CaO}} \rho V \quad (2)$$

,

where C_{sample} is the carbon content (g), x_{CaO} is the CaO content (wt%), ρ is the specific gravity (g cm^{-3}), and V is the volume (cm^3) of the sample.

When we apply the values listed in Table 5 to the equation above, the carbon content in the glendonite concretion from the Asagai Formation (Fig. 5a) is approximately 37.5 g. The volume of the glendonite concretion was obtained from the concretion's 3D morphological data. The calculation assumes that the glendonite occupies half of the concretion's volume, and Cal-1—granular calcite derived from ikaite—occupies 31.4% of the glendonite (Shearman and Smith, 1985), and they comprise pure calcite. Glendonite concretions from the Asagai Formation do not contain carbonates other than calcite (Fig. 8). CaO is also contained in the sediments in the concretion; therefore, this estimation is the maximum amount.

The bivalve carbon content in the glendonite concretion can be estimated as 2.0 g, assuming that the bivalve volume is 30 cm^3, the bivalve contains 6.2 wt% carbon in their wet soft tissue (Brey et al., 2010), and the specific gravity is 1.1 g cm^{-3} [using human body density (Durnin and Womersley, 1974)].

The carbon content of the glendonite concretion, which exceeds the expected amount in dead organisms, indicates that organic matter in sediments and organic carbon remaining as ichnofossils could have supplied bicarbonate to form glendonite concretions.

However, organic matter in sediments, i.e., external carbon sources, alone cannot explain the spherical shape of concretions because outward diffusion of bicarbonate from the center of the concretions is required to form spherical concretions (Yoshida et al., 2015, 2018, 2020). The explanation that concretions grew by nucleating on ikaite crystals is ruled out because the glendonite terminations are thrust out of the concretion surfaces (Fig. 1). If concretions grew by nucleating ikaite crystals, the concretion should completely encase the glendonites. Also, if the carbon sources for ikaite crystals and the surrounding concretions were different, i.e., organic matter in sediments supplied bicarbonate to form ikaite crystals and dead organisms provided for the surrounding concretions, concretions would be very unlikely to form specifically around the ikaite crystals. The dissolved inorganic carbon in seawater might also have contributed to forming glendonite concretions; however, the negative $\delta^{13}C$ values of the glendonite concretions indicate that the amount was small (Fig. 15, Table 4) because carbonates derived from inorganic carbon in seawater have $\delta^{13}C$ values of approximately 0‰ (Nelson and Smith, 1996). Therefore, glendonite concretions formed using bicarbonate supplied from dead organisms with the aid of organic matter in the surrounding sediments. Glendonite concretions formed in fossil-poor strata can be explained by the contribution of soft-bodied organisms, which are rarely preserved as fossils. This interpretation is supported by the fact that most glendonite concretions are found in bioturbated mudstone, indicating the abundant existence of benthic organisms.

The occurrence, $\delta^{13}C$ values, and P concentrations of glendonite concretions and glendonites without concretions show that both ikaite and the surrounding concretions formed from bicarbonate, generated by the decomposition of dead organisms' soft tissue and organic matter in sediments. Microorganisms perform organic decomposition in

sediments through several reaction pathways (Froelich et al., 1979). The blue-gray of the fresh part of the host mudstone and concretions indicate the reduced sediment environments. Sulfate reduction is a primary organic decomposition process in a reduced environment; however, it decreases porewater pH due to H^+ generation and is inefficient for carbonate precipitation unless sulfide is precipitated (Soetaert et al., 2007; Meister, 2013). Also, the small amount of pyrite in the concretions indicates that the organic decomposition by sulfate reduction was not the primary process during glendonite concretion formation. Anoxic oxidation of methane (AOM) induces carbonate precipitation (Peckmann and Thiel, 2004); however, its characteristic highly reduces the $\delta^{13}C$ values [e.g., −56‰ to −35‰ (Stakes et al., 1999)] and are not recognized in the glendonite concretions of this study. Manganese and iron reduction increases pH by consuming H^+ (Soetaert et al., 2007), and the reactions are intensified in highly bioturbated sediments (Burdige, 1993; Canfield et al., 1993; Quintana et al., 2015). Although lacking a direct index, considering the highly bioturbated facies of the glendonite concretion-bearing strata, these organic decomposition pathways played a significant role in forming the glendonite concretions. During the decomposition, bicarbonate from decaying organisms reacted with Ca ions in the porewater, forming an ikaite crystal and a concretion around an ikaite crystal.

4-3. The growth rate and formation environment of glendonite concretion

Ca distribution in and around the glendonite concretion (Fig. 12) shows sharp margin characterized as the “reaction front”, typically observed in rapidly formed calcite concretions (Yoshida et al., 2015, 2018, 2019, 2020). The near homogeneous Ca distribution and concentration decreasing at the concretion margin result from reactions

with bicarbonate diffusing out from the concretion's central part, with Ca ions in the porewater of surrounding sediments (Yoshida et al., 2015, 2018, 2020).

When we adopt this growth model, the concretion growth rate formed by this outward diffusion process can be estimated from the reaction-front width and the "diffusion-growth rate cross plot" (Yoshida et al., 2015, 2018, 2020). Several measured concretions around glendonite with a 3–10 cm diameter have 2–8-mm reaction-front widths (Fig. 12). The width applied in the diffusion-growth rate cross plot indicates that the concretion around glendonite was formed over several months to years. Bending laminae in the matrixes around glendonite concretions (Fig. 1h) and undeformed ichnofossils in concretions also show that the concretion formation was completed early in the deposition before the sediment compaction. This is also consistent with the estimated formation depth of modern ikaite crystals, i.e. <10 m (Lu et al., 2012; Kakuwa et al., 2019; Hiruta and Matsumoto, 2022).

The $\delta^{18}O$ values of concretions around glendonites indicate that concretions formed in a shallow part of the sediments, and the average $\delta^{18}O$ value is approximately 0‰ (Fig. 15), except for concretions from the Asagai Formation, which likely underwent meteoric alteration on the outcrop. Most $\delta^{18}O$ values of concretions are similar to those of bivalve shells (Fig. 15 and Table 4). In most cases, such biogenic carbonates precipitated in isotopic equilibrium with seawater (Bickert, 2006), indicating that concretions around ikaite crystals formed from porewater with $\delta^{18}O$ values similar to seawater, which could exist in sediments near the seafloor.

Bulk glendonites in concretions comprise three phases of carbonates, but Cal-1 and Cal-2 occupy more than 90% of the volume (Fig. 7). The similarities in the $\delta^{18}O$ values of Cal-1, bulk glendonites in concretions from the Morai and Toyohama formations, and

shell fossils (Fig. 15) indicate that the ikaite transformation and Cal-2 cementation also occurred near the sediment surfaces.

Ikaite is formed in various environments, such as organic-rich marine sediments and submarine or terrestrial springs (e.g., Pauly, 1963; Suess et al., 1982; Ito, 1996). The factors controlling ikaite formation must consider each environment's physicochemical characteristics. It has been experimentally shown that high phosphate concentrations promote ikaite precipitation at pH 9.0 (Hu et al., 2015), stabilize ikaite, and increase the time to the conversion of ikaite to vaterite and calcite (Bischoff et al., 1993). This could be because phosphate inhibits the precipitation of more stable phases of calcium carbonate, such as calcite and aragonite (Bischoff et al., 1993). Several studies have reported high phosphate concentrations greater than 100 μM (its concentration in normal seawater is approximately 2 μM; Nozaki, 2001) in the porewater of marine sediments at several localities where ikaite crystals are formed (Kodina et al., 2003; Zhou et al., 2015).

Mg^{2+} concentrations as high as those in seawater also favor ikaite precipitation around pH 10 or higher, typical of alkaline spring environments (Stockmann et al., 2018; Tollefsen et al., 2018). Kakuwa et al. (2019) showed that Mg^{2+} concentrations in the porewater of marine sediments are similar in marine sediments with and without ikaite crystals, indicating that Mg^{2+} concentrations alone are not a controlling factor in ikaite formation in marine sediments. Fe^{2+} and Mn^{2+} also inhibit calcite growth (Meyer, 1984), and their concentrations in the porewater increase during organic decomposition, accompanied by reductions in Fe and Mn oxides (Jørgensen and Kasten, 2006). If Mg^{2+}, Fe^{2+}, and/or Mn^{2+} in the porewater are the only factors controlling ikaite crystal formation in marine sediments, it is difficult to explain the limited findings of ikaite crystals in marine sediments.

XRF analyses of the glendonites and the surrounding concretions show high P concentrations of approximately 1 wt%, 2–16 times higher than that of the matrixes (Table 2). Conversely, the Mg, Fe, and Mn concentrations in the glendonites and concretions are at the same level as those in the matrixes (Table 2) and average shales globally (Gromet et al., 1984). Although the Mg^{2+}, Fe^{2+}, and Mn^{2+} contributions could not be completely ruled out, the high P concentrations in glendonite concretions imply that the high phosphate environment generated by the decomposition of dead organisms plays a vital role during glendonite concretion formation.

EPMA analyses show the selective P distribution in glendonite concretions (Fig. 14). P concentrates in the concretions around glendonites and Cal-2 as calcium phosphate inclusions (Table 3); however, almost no P is detected in Cal-1 (ikaite-derived calcite). This selective P distribution is also shown in glendonites from Sakhalin Island and the Barents Shelf of Russia (Mikhailova et al., 2021; Vasileva et al., 2021). Considering that high phosphate concentrations favor the ikaite formation, this P distribution indicates that phosphate generated from decomposing dead organisms was dissolved during ikaite formation to favor ikaite precipitation. After ikaite formation, it precipitated as calcium phosphate inclusions to be incorporated into Cal-2 and concretions. Because ikaite incorporates no phosphate during precipitation (Hu and Wang, 2020), the absence of P in Cal-1 is not contradicted a high phosphate environment during ikaite formation. When the phosphate concentration in the porewater falls below the ikaite stabilization threshold due to calcium phosphate precipitation, fine calcite crystals begin to precipitate by consuming the remaining bicarbonate around an ikaite crystal, forming spherical calcite concretions (Muramiya et al., 2022).

Phosphate adsorption/desorption on/from ferric iron minerals and the formation of

authigenic phosphate minerals change the phosphate concentrations in porewater. The phosphate concentration occurring as calcium phosphate inclusions in glendonite concretions (Fig. 14, Table 3) indicates that the precipitation of authigenic phosphate minerals changes the phosphate concentration during glendonite concretion formation. Because pH significantly affects phosphate solubility (Macha et al., 2015), the phosphate concentration could be controlled by porewater pH, determined by the balance between the organic acid generation during organic decomposition and the buffering effect of seawater. Assuming that the porewater pH trend of ancient marine sediments is the same as that of modern marine sediments (7–8) (Shao et al., 2016), glendonite concretions were presumably formed under these pH conditions. Kodina et al. (2003) supported this assumption, reporting that the porewater pH of marine sediments containing ikaite crystals was 7–8.

4-4. The formation process of glendonite concretion

Previously, concretions enclosing glendonites were thought to have formed after ikaite transformation to calcite (Qu et al., 2017; Vickers et al., 2020; Vasileva et al., 2021). However, observations of the glendonite surface structures in this study show that concretion had been formed before the ikaite transformation. When ikaite crystals transform into aggregations of granular calcite, the aggregation surface becomes rough (Jansen et al., 1987; Tollefsen et al., 2020). The rough surfaces of glendonites without concretions (Fig. 7e, f) show that the transformation of ikaite crystals in unconsolidated sediments caused the surrounding sediments to intrude into the pores distributed on the granular calcite aggregation. In contrast, the smooth surfaces of glendonites in concretions (Fig. 7a, b) show that concretions formed to consolidate around ikaite crystals

before the transformation, preventing the physical disturbance of the surrounding sediments. The bend laminae around the concretions also indicate the formation of concretions in unconsolidated sediments (Fig. 1h).

Figure 16 summarizes the sequential process from ikaite crystallization to concretion formation and the related geochemical changes due to decomposing dead organisms. This formation scenario for glendonite concretions can account for variations in the relative glendonite sizes to the surrounding concretions (Fig. 1). The timing of changes in phosphate concentrations in porewater determines the carbon proportion in the dead organisms used to form ikaite. For example, when the phosphate concentration was maintained at a high level until the late phase of decomposition, most carbon in the dead organisms will have been used for ikaite crystal growth; therefore, glendonite would be moderately large to concretion (Fig. 1g). If the phosphate concentration was maintained high throughout the decomposition process, all carbon would have been consumed to form ikaite crystals (the case of glendonites without concretions: Fig. 1j–l). In contrast, when the phosphate concentration decreased in an early phase of decomposition, only a tiny amount of carbon will have been used for ikaite crystal growth, and glendonite would be small to concretion (Fig. 1i). If the phosphate concentration in porewater was maintained at a low level throughout the decomposition process, all the carbon in the dead organisms would have been consumed to precipitate calcite that forms concretions. Also, if the temperature was too high for ikaite to stabilize, all the carbon in the dead organisms would have been consumed to form concretions. This formation process shows that glendonite concretions indicate changes in the phosphate concentration, presumably controlled by porewater pH during early diagenesis (Fig. 16) (Muramiya et al., 2022).

4-5. Implications of glendonite concretion for understanding early diagenesis

Early diagenesis is crucial for recording much information on the paleoenvironment in sedimentary rocks as chemical and isotopic compositions of authigenic minerals. The early diagenesis process has been studied for many years, and details are becoming clearer, especially from studies on carbonate concretions (e.g., Irwin et al., 1977; Matsumoto and Iijima, 1981; Carpenter et al., 1988; Coleman, 1993; Nelson and Smith, 1996; Hudson et al., 2001; Hendry et al., 2006; Alessandretti et al., 2015).

Although porewater pH is a significant parameter that controls the solubility and speciation of various substances (Chuan et al., 1996; Grasby and Schulz, 1999; Liu and Millero, 2002; Macha et al., 2015), affecting the elemental cycle and mineral formation in early diagenesis, it has been difficult to determine. This study revealed the detailed formation process of glendonite concretions and showed for the first time that the relative size of glendonites to surrounding concretions indicates porewater pH changes during early diagenesis. Therefore, glendonite concretions can provide us with essential information for understanding the geochemical process of early diagenesis.

The formation conditions of glendonites have been investigated from glendonites in sedimentary rocks and natural or synthetic crystals of ikaite (e.g., Suess et al., 1982; Teichert and Luppold, 2013; Zhou et al., 2015; Vickers et al., 2018; Tollefsen et al., 2020). This study's results show the importance of porewater pH on glendonite concretion formation; however, the effects of other factors, such as Mg^{2+} concentrations, are still under consideration. A detailed understanding of their formation conditions will further clarify the usefulness of glendonites and glendonite concretions as geochemical indicators.

Chapter 5. Conclusions

A literature survey, geological investigation and observations, and geochemical analyses revealed the formation process and environments of glendonite concretions. For the geological investigation, four sedimentary strata in Japan were chosen: middle to late Eocene Poronai Formation, Mikasa, Hokkaido; late Miocene Morai Formation, Ishikari, Hokkaido; early Oligocene Asagai Formation, Iwaki, Fukushima; and early Miocene Toyohama Formation, Minamichita, Aichi.

The compiled information on glendonites in Japan shows that at least 36 formations yield glendonites. Most formations comprised gray to black muddy rocks and were deposited on the seafloor at depths of several hundred meters, indicating that ikaite crystals tend to form in organic-rich marine sediments under low temperatures. Glendonite concretions were recognized in 19 formations within all glendonite identified formations, and their temporal and spatial distributions are similar within their distribution. Therefore, glendonite concretion formation is not a peculiar case to a specific region or geologic age.

Glendonite concretions from the Asagai Formation contain articulated bivalves at the center, and those from the other formations contain fossils such as crustaceans and ichnofossils. Glendonites and the surrounding concretions have negative $\delta^{13}C$ values and high phosphate concentrations. The occurrence and geochemistry of glendonite concretions show that they were formed from organic carbon in dead organisms and organic matter in sediments. The phosphate distribution in glendonite in concretions indicates that changes in phosphate concentrations, controlled by porewater pH, determined the timing of the growth termination of ikaite crystals and the start of the

formation of surrounding concretion. Bending laminae around concretions, undeformed ichnofossils, Ca distributions, and $\delta^{18}O$ values show that concretion formation was completed in a shallow part of sediments within months to years. This formation process could be applied to determine the change in porewater pH during early diagenesis. Porewater pH is a significant parameter controlling the mineral formation in early diagenesis; therefore, this study provides essential information for understanding early diagenesis.

Acknowledgments

I am indebted to H. Yoshida, M. Takeuchi, K. Tsukada, T. Oji, S. Nishida, S. Kadowaki, S. Fujiwara, and all TEGED and Museum Seminar members of Nagoya University for useful discussions. I am grateful to K. Yamamoto, Y. Asahara, M. Minami, A. Ikeda, A. Umemura, R. Kuma of Nagoya University, and N. Katsuta of Gifu University for their support in the geochemical analyses. I thankfully acknowledge M. Ikehara, T. Komatsu, and Y. Fujimura of Kochi University for providing me with equipment for the stable isotope analyses. I wish to thank Y. Yamamoto and T. Matsuzaki of Kochi University for providing me with equipment for the EPMA analyses. I would also like to thank S. Yogo and N. Takagi of Nagoya University for preparing samples. S. Nishimoto of Nagoya City Science Museum gave me insightful comments on XRD analyses. H. Hasegawa of Kochi University gave me useful comments on the interpretation of geologic data. A. Ujihara of Nagoya University and T. Mikami of the University of Tokyo help me during field investigations. T. Ohmi of Hokkaido University, H. Kokubun of Mikasa City, K. Moriki, J. Sekikawa, T. Tsuji, K. Fukuda of Sapporo City, S. Nabana of Iwakishi

sekitan kasekikan, T. Kobayashi of Iwaki Sogo High School and K. Sekiuchi of the Iwaki Regional Science Association provide us valuable samples and information. M. Rogov of Geological Institute RAS provided me with references that are difficult to obtain. Taira-Mokuzai-Ichiba provided a permit to conduct geological investigations and sampling on their private land. The isotopic analyses and EPMA analyses at Kochi University were performed under the cooperative research program of the Center for Advanced Marine Core Research (CMCR), Kochi University (19B068, 20C002).

References

Alessandretti, L., Warren, L.V., Machado, R., Novello, V.F., Sayeg, I.J., 2015, Septarian carbonate concretions in the Permian Rio do Rasto Formation: birth, growth and implications for the early diagenetic history of southwestern Gondwana succession. Sedimentary Geology 326, 1–15.

Baird, G.C., Sroka, S.D., Shabica, C.W., Kuecher, G.J., 1986, Taphonomy of Middle Pennsylvanian Mazon Creek Area fossil localities, northeast Illinois: significance of exceptional fossil preservation in syngenetic concretions. Palaios 1, 271–285.

Baucon, A., Bednarz, M., Dufour, S., Felletti, F., Malgesini, G., Neto de Carvalho, C., Niklas, K.J., Wehrmann, A., Batstone, R., Bernardini, F., Briguglio, A., Cabella, R., Cavalazzi, B., Ferretti, A., Zanzerl, H., McIlroy, D., 2020, Ethology of the trace fossil *Chondrites*: form, function and environment. Earth-Science Reviews 202, 102989.

Bickert, T., 2006, Influence of geochemical processes on stable isotope distribution in marine sediments. in: Schulz, H.D. and Zabel, M. (Eds.), Marine Geochemistry,

Springer, Berlin, pp. 339–360.

Bischoff, J.L., Fitzpatrick, J.A., Rosenbauer, R.J., 1993, The solubility and stabilization of ikaite ($CaCO_3 \cdot 6H_2O$) from 0° to 25°C: environmental and paleoclimatic implications for thinolite tufa. Journal of Geology 101, 21–33.

Boggs Jr, S., 1972, Petrography and geochemistry of rhombic, calcite pseudomorphs from Mid-Tertiary mudstones of the Pacific Northwest, U.S.A. Sedimentology 19, 219–235.

Brey, T., Müller-Wiegmann, C., Zittier, Z.M.C., Hagen, W., 2010. Body composition in aquatic organisms—A global data bank of relationships between mass, elemental composition and energy content. Journal of Sea Research 64, 334–340.

Buchardt, B., Seaman, P., Stockmann, G., Vous, M., Wilken, U., Düwel, L., Kristiansen, A., Jenner, C., Whiticar, M.J., Kristensen, R.M., Peterson, G.H., Thorbjørn, L., 1997, Submarine columns of ikaite tufa. Nature 390, 129–130.

Burdige, D.J., 1993. The biogeochemistry of manganese and iron reduction in marine sediments. Earth Science Reviews 35, 249–284.

Burton, E.A., 1993, Controls on marine carbonate cement mineralogy: review and reassessment. Chemical Geology 105, 163–179.

Canfield, D.E., Thamdrup, B., Hansen, J.W., 1993, The anaerobic degradation of organic matter in Danish coastal sediments: Iron reduction, manganese reduction, and sulfate reduction. Geochimica et Cosmochimica Acta 57, 3867–3883.

Carpenter, S.J., Erickson, J.M., Lohmann, K.C., Owen, M.R., 1988, Diagenesis of fossiliferous concretions from the Upper Cretaceous Fox Hills Formation, North Dakota. Journal of Sedimentary Petrology 58, 706–723.

Chuan, M.C., Shu, G.Y., Liu, J.C., 1996, Solubility of heavy metals in a contaminated

soil: effects of redox potential and pH. Water, Air, and Soil Pollution 90, 543–556.

Clements, T., Purnell, M., Gabbott, S., 2019, The mazon creek lagerstätte: A diverse late paleozoic ecosystem entombed within siderite concretions. Journal of the Geological Society 176, 1–11.

Coleman, M.L., 1993, Microbial processes: Controls on the shape and composition of carbonate concretions. Marine Geology 113, 127–140.

Craig, H., 1957. Isotopic standards for carbon and oxygen and correction factors for mass-spectrometric analysis of carbon dioxide. Geochimica et Cosmochimica Acta 12, 133–149.

Curtis, C.D., Coleman, M.L., Love, L.G., 1986, Pore water evolution during sediment burial from isotopic and mineral chemistry of calcite, dolomite and siderite concretions. Geochimica et Cosmochimica Acta 50, 2321–2334.

Dale, A., John, C.M., Mozley, P.S., Smalley, P.C., Muggeridge, A.H., 2014, Time-capsule concretions: unlocking burial diagenetic processes in the Mancos Shale using carbonate clumped isotopes. Earth and Planetary Science Letters 394, 30–37.

De Lurio, J.L., Frakes, L.A., 1999, Glendonites as a paleoenvironmental tool: Implications for early Cretaceous high latitude climates in Australia. Geochimica et Cosmochimica Acta 63, 1039–1048.

Dieckmann, G.S., Nehrke, G., Uhlig, C., Göttlicher, J., Gerland, S., Granskog, M.A., Thomas, D.N., 2010, Brief communication: ikaite ($CaCO_3 \cdot 6H_2O$) discovered in Arctic sea ice. The Cryosphere 4, 227–230.Drever, J.I., 1997, The geochemistry of natural waters: surface and groundwater environments. Prentice Hall, Hoboken, NJ, 436p.

Durnin, J.V.G.A., Womersley, J., 1974, Body fat assessed from total body density and

its estimation rrom skinfold thickness: easurements on 481 men and women aged from 16 to72 years. British Journal of Nutrition 32, 77–97.

Editorial Committee of HOKKAIDO, Part 1 of Regional Geology of Japan, 1990, Regional geology of Japan, Part 1, HOKKAIDO. Kyoritsu Shuppan, pp. 337.

Frank, T.D., Thomas, S.G., Fielding, C.R., 2008, On using carbon and oxygen isotope data from glendonites as paleoenvironmental proxies: a case study from the Permian system of eastern Australia. Journal of Sedimentary Research 78, 713–723.

Froelich, P.N., Klinkhammer, G.P., Bender, M.L., Luedtke, N.A., Heath, G.R., Cullen, D., Dauphin, P., Hammond, D., Hartman, B., Maynard, V., 1979, Early oxidation of organic matter in pelagic sediments of the eastern equatorial Atlantic: suboxic diagenesis. Geochimica et Cosmochimica Acta 43, 1075–1090.

Glasby, G.P., Schulz, H.D., 1999, EH, pH diagrams for Mn, Fe, Co, Ni, Cu and As under seawater conditions: application of two new types of EH, pH diagrams to the study of specific problems in marine geochemistry. Aquatic Geochemistry 5, 227–248.

Grasby, S.E., McCune, G.E., Beauchamp, B., Galloway, J.M., 2017, Lower Cretaceous cold snaps led to widespread glendonite occurrences in the Sverdrup Basin, Canadian High Arctic. Bulletin of the Geological Society of America 129,

Greinert, J., Derkachev, A., 2004, Glendonites and methane-derived Mg-calcites in the Sea of Okhotsk, Eastern Siberia: implications of a venting-related ikaite/glendonite formation. Marine Geology 204, 129–144.

Gromet, L.P., Haskin, L.A., Korotev, R.L., Dymek, R.F., 1984, The “North American shale composite”: Its compilation, major and trace element characteristics.

Geochimica et Cosmochimica Acta 48, 2469–2482.

Hendry, J.P., Pearson, M.J., Trewin, N.H., Fallick, A.E., 2006, Jurassic septarian concretions from NW Scotland record interdependent bacterial, physical and chemical processes of marine mudrock diagenesis. Sedimentology 53, 537–565.

Hensen, C., Zabel, M., Schulz, H, 2006, Benthic cycling of oxygen, nitrogen and phosphorus, in: Schulz, H.D. and Zabel, M. (Eds.), Marine Geochemistry, Springer, Berlin, pp. 207–240.

Hertweck, G., Wehrmann, A., Liebezeit, G., 2007, Bioturbation structures of polychaetes in modern shallow marine environments and their analogues to *Chondrites* group traces. Palaeogeography, Palaeoclimatology, Palaeoecology 245, 382–389.

Hiruta, A., Matsumoto, R., 2022, Geochemical comparison of ikaite and methane-derived authigenic carbonates recovered from Echigo Bank in the Sea of Japan. Marine Geology 443, 106672.

Hu, Y.-B., Wang, F., 2020, Effect of ikaite precipitation on phosphate removal in sea ice. Polar Research 39, 3413.

Hu, Y.-B., Wolthers, M., Wolf-Gladrow, D.A., Nehrke, G., 2015, Effect of pH and phosphate on calcium carbonate polymorphs precipitated at near-freezing temperature. Crystal Growth and Design 15, 1596–1601.

Hudson, J.D., Coleman, M.L., Barreiro, B.A., Hollingworth, N.T.J., 2001, Septarian concretions from the Oxford Clay (Jurassic, England, UK): involvement of original marine and multiple external pore fluids. Sedimentology 48, 507–531.

Huggett, J.M., Schultz, B.P., Shearman, D.J., Smith, A.J., 2005, The petrology of ikaite pseudomorphs and their diagenesis. Proceedings of the Geologists' Association

116, 207–220.

Irwin, H., Curtis, C., Coleman, M., 1977, Isotopic evidence for source of diagenetic carbonates formed during burial of organic-rich sediments. Nature 269, 209–213.

Ito, C., Irizuki, T., Iwai, M., 1999, Diatom zonal key species and geologic ages of the Miocene Morozaki, Iwamura and Tomikusa Groups in the First Setouchi Province, central Japan. The Journal of the Geological Society of Japan 105, 152–155.

Ito, T., 1996, Ikaite from cold spring water at Shiowakka, Hokkaido, Japan. Journal of Mineralogy, Petrology and Economic Geology 91, 209–219.

Ito, Y., Yoshida, T., Harima, C., 2015, Estimation of diets and food sources of juvenile marbled sole in Sengan Bay, Seto Inland Sea, Japan, based on carbon and nitrogen stable isotope ratios. Nippon Suisan Gakkaishi 81, 681–687.

Jansen, J.H.F., Woensdregt, C.F., Kooistra, M.J., van der Gaast, S.J., 1987, Ikaite pseudomorphs in the Zaire deep-sea fan: an intermediate between calcite and porous calcite. Geology 15, 245–248.

Jauvion, C., Audo, D., Bernard, S., Vannier, J., Daley, A.C., Charbonnier, S., 2020, A new polychelidan lobster preserved with its eggs in a 165 Ma nodule. Scientific Reports 10, 3574.

Jones, A.T., Frank, T.D., Fielding, C.R., 2006, Cold climate in the eastern Australian mid to late Permian may reflect cold upwelling waters. Palaeogeography, Palaeoclimatology, Palaeoecology 237, 370–377.

Jørgensen, B.B., 2006, Bacteria and marine biogeochemistry, in: Schulz, H.D., Zabel, M. (Eds.), Marine Geochemistry. Springer, Berlin, pp. 169–206.

Jørgensen, B.B., Kasten, S., 2006, Sulfur Cycling and Methane Oxidation, in: Schulz, H.D., Zabel, M. (Eds.), Marine Geochemistry. Springer, Berlin, pp. 271–310.

Kaiho, K., 1984, Tertiary stratigraphy of the Yubari district, central Hokkaido, Japan. The Journal of Geological Society of Japan 90, 815–829.

Kakuwa, Y., Zhang, N., Matsumoto, R., Tomaru, H., Ishida, N., Motegi, T., 2019, The discovery of ikaite from sediment cores in the eastern margin of the Japan Sea and its significance. The Journal of the Geological Society of Japan 125, 853–865.

Katsuta, N., Takano, M., Okaniwa, T., Kumazawa, M., 2003, Image processing to extract sequential profiles with high spatial resolution from the 2D map of deformed laminated patterns. Computers and Geosciences 29, 725–740.

Kim, S.T., O'Neil, J.R., 1997, Equilibrium and nonequilibrium oxygen isotope effects in synthetic carbonates. Geochimica et Cosmochimica Acta 61, 3461–3475.

Kodama, M., Watanabe, S., Yagi, H., Nadaoka, K., Suzuki, N., Furutono, T., 2011, Temporal variability of carbon and nitrogen stable isotopes of bivalves in Tamagawa River estuary, Japan. Journal of Japan Society of Civil Engineers, Ser. B2 (Coastal Engineering) 67, 961–965.

Kodina, L.A., Tokarev, V.G., Vlasova, L.N., Korobeinik, G.S., 2003, Contribution of biogenic methane to ikaite formation in the Kara Sea: evidence from the stable carbon isotope geochemistry, in: Stein, R., Fahl, K., Fütterer, D.K., Galimov, E.M., Stepanets, O. V. (Eds.), Siberian River Run-off in the Kara Sea: Characterisation, Quantification, Variability and Environmental Significance. Elsevier, Amsterdam, pp. 349–374.

Koot, M. B., 2013, Effects of the late Permian mass extinction on chondrichthyan palaeobiodiversity and distribution patterns.

Krom, M.D., Berner, R.A., 1981, The diagenesis of phosphorus in a nearshore marine sediment. Geochimica et Cosmochimica Acta 45, 207–216. Copenhagen,

University of Copenhagen, Ph. D. thesis.

Landman, N.H., Klofak, S.M., 2012, Anatomy of a concretion: life, death, and burial in the Western Interior Seaway. Palaios 27, 671–692.

Liu, X., Millero, F.J., 2002, The solubility of iron in seawater. Marine Chemistry 77, 43–54.

Lu, Z., Rickaby, R.E.M., Kennedy, H., Kennedy, P., Pancost, R.D., Shaw, S., Lennie, A., Wellner, J., Anderson, J.B., 2012, An ikaite record of late Holocene climate at the Antarctic Peninsula. Earth and Planetary Science Letters 325–326, 108–115.

Macha, I.J., Boonyang, U., Cazalbou, S., Ben-Nissan, B., Charvillat, C., Oktar, F.N., Grossin, D., 2015, Comparative study of coral conversion, Part 2: Microstructural evolution of calcium phosphate. Journal of the Australian Ceramic Society 51, 149–159.

Maeda, H., Shigeta, Y., 2005, Maastrichtian Ammonoid Fauna from the Pugachevo Area, Southern Sakhalin, Russian Far East. National Science Museum Monographs 31, 121–136.

Marshall, J.D., Pirrie, D., 2013, Carbonate concretions—explained. Geological Today 29, 53–62.

Martill, D.M., 1988, Preservation of fish in the Cretaceous Santana Formation of Brazil. Palaeontology 31, 1–18.

Matsumoto, R., Iijima, A., 1981, Origin and diagenetic evolution of Ca-Mg-Fe carbonates in some coalfields of Japan. Sedimentology 28, 239–259.

Matsuno, K., Tanaka, K., Mizuno, A., Ishida, M., 1964, Geology of the Iwamizawa district. Quadrangle Series, 1:50,000. Geological Survey of Japan.

Meister, P., 2013, Two opposing effects of sulfate reduction on carbonate precipitation

in normal marine, hypersaline, and alkaline environments. Geology 41, 499–502.

Meyer, H.J., 1984, The influence of impurities on the growth rate of calcite. Journal of Crystal Growth 66, 639–646.

Mikhailova, K., Rogov, M., Ershova, V., Vereshchagin, O., Shurekova, O., Feodorova, A., Zakharov, V., 2021, Middle Jurassic–Lower Cretaceous glendonites from the eastern Barents Shelf as a tool for paleoenvironmental and paleoclimatic reconstructions. Palaeogeography, Palaeoclimatology, Palaeoecology 579, 110600.

Morikiyo, T., Morita, R., Furuhashi, S., 2018, Glendonite-bearing calcareous nodules from the mudstone of the Araya Formation in the Tochio area, Niigata Prefecture. Earth Science 72, 195–211.

Mozley, P.S., Burns, S.J., 1993, Oxygen and carbon isotopic composition of marine carbonate concretions: an overview. Journal of Sedimentary Petrology 63, 73–83.

Muramiya, Y., Ujihara, A., Oji, T., Yoshida, H., 2020, Spherical carbonate concretions and deep-sea fossils in the Miocene Morozaki Group, Chita Peninsula, central Japan. The Journal of the Geological Society of Japan 126, 355–363.

Muramiya, Y., Yoshida, H., 2020, Glendonite and “glendonite concretion” in Japan: sedimentary environment of glendonite-bearing strata. Annual Report of Fukada Geological Institute 21, 47–58.

Muramiya, Y., Yoshida, H., A review of the occurrence and the origin of glendonite and glendonite concretion. The Journal of the Geological Society of Japan, submitted.

Muramiya, Y., Yoshida, H., Kubota, K., Minami, M., 2020, Rapid formation of gigantic spherical dolomite concretion in marine sediments. Sedimentary Geology 404, 105664.

Muramiya, Y., Yoshida, H., Minami, M., Mikami, T., Kobayashi, T., Sekiuchi, K.,

Katsuta, N., 2022, Glendonite concretion formation due to dead organism decomposition. Sedimentary Geology 429, 106075.

Muramiya, Y., Yoshida, H., Yamamoto, K., Minami, M., 2017, Formation of gigantic spherical carbonate concretion in early diagenesis. The Journal of the Geological Society of Japan 123, 939–952.

Nakashima, S., Yamada, Y., Tada, K., 2007, The carbon and nitrogen stable isotope ratios of the fishes in the coastal area of Kagawa Prefecture. Technical bulletin of Faculty of Agriculture, Kagawa University 59, 59–64.

Nelson, C.S., Smith, A.M., 1996, Stable oxygen and carbon isotope compositional fields for skeletal and diagenetic components in New Zealand Cenozoic nontropical carbonate sediments and limestones: A synthesis and review. New Zealand Journal of Geology and Geophysics 39, 93–107.

Nire, K., 1934, Hokoseki from the Rikuzen district, Miyagi, Japan. Our Minerals 3, 10–14.*

Nogoshi, O., 1966, Hokoseki from the Tertiary of the Sunago-sawa River, Yamagaya, Japan. Chigaku Kenkyu 17, 150–151.*

Nozaki, Y., 2001, Elemental distribution/ overview, in: Steele, J.H. (Ed.), Encyclopedia of Ocean Sciences. Elsevier, Amsterdam, pp. 840–845.

Ogasawara, K., Kubo, K., Nakano, T., Uemura, K., 2001, Evaluation of Sr isotopic dating using shell fossils, in: Reconstruction of Sedimentary Environments in the Lower Miocene of Honshu, Japan. pp. 27–29.*

Okada, H., Kaiho, K., 1992, Paleogene calcareous nannofossils from Hokkaido, Japan., in: Ishizaki, K., Saito, T. (Eds.), Centenary of Japanese Micropaleontology. Terra Scientific Publishing Company, Tokyo, pp. 461–471.

Pauly, H., 1963, "Ikaite", a new mineral from Greenland. Arctic 16, 263–264.

Peckmann, J., Thiel, V., 2004, Carbon cycling at ancient methane-seeps. Chemical Geology 205, 443–467.

Plet, C., Grice, K., Pagès, A., Verrall, M., Coolen, M.J.L., Ruebsam, W., Rickard, W.D.A., Schwark, L., 2017, Palaeobiology of red and white blood cell-like structures, collagen and cholesterol in an ichthyosaur bone. Scientific Reports 7, 13776.

Popov, L.E., Álvaro, J.J., Holmer, L.E., Bauert, H., Ghobadi Pour, M., Dronov, A. V., Lehnert, O., Hints, O., Männik, P., Zhang, Zhifei, Zhang, Zhiliang, 2019, Glendonite occurrences in the Tremadocian of Baltica: first Early Palaeozoic evidence of massive ikaite precipitation at temperate latitudes. Scientific Reports 9, 7205.

Price, G.D., 1999, The evidence and implications of polar ice during the Mesozoic. Earth Science Reviews 48, 183–210.

Qu, Y., Teichert, B.M.A., Birgel, D., Goedert, J.L., Peckmann, J., 2017, The prominent role of bacterial sulfate reduction in the formation of glendonite: a case study from Paleogene marine strata of western Washington State. Facies 63, 10.

Quintana, C.O., Shimabukuro, M., Pereira, C.O., Alves, B.G.R., Moraes, P.C., Valdemarsen, T., Kristensen, E., Sumida, P.Y.G., 2015, Carbon mineralization pathways and bioturbation in coastal Brazilian sediments. Scientific Reports 5, 16112.

Rogov, M., Ershova, V., Vereshchagin, O., Vasileva, K., Mikhailova, K., Krylov, A., 2021, Database of global glendonite and ikaite records throughout the Phanerozoic. Earth System Science Data 13, 343–356.

Rogov, M.A., Ershova, V.B., Shchepetova, E. V., Zakharov, V.A., Pokrovsky, B.G., Khudoley, A.K., 2017, Earliest Cretaceous (late Berriasian) glendonites from Northeast Siberia revise the timing of initiation of transient Early Cretaceous cooling in the high latitudes. Cretaceous Research 71, 102–112.

Rogov, M.A., Zakharov, V.A., 2010, Jurassic and Lower Cretaceous glendonite occurrences and their implication for Arctic paleoclimate reconstructions and stratigraphy. Earth Science Frontiers 17, 345–347.

Sagayama, T., 2003, Geologic age of the boundary part between the Embetsu Formation-Koetoi Formation and the Yuchi Formation, northern Hokkaido, Japan: Rubeshube River and Kaminukanan River routes. The Journal of Geological Society of Japan 109, 310–323.

Selleck, B.W., Carr, P.F., Jones, B.G., 2007, A review and synthesis of glendonites (pseudomorphs after ikaite) with new data: Assessing applicability as recorders of ancient coldwater conditions. Journal of Sedimentary Research 77, 980–991.

Shao, C., Sui, Y., Tang, D., Legendre, L., 2016, Spatial variability of surface-sediment porewater pH and related water-column characteristics in deep waters of the northern South China Sea. Progress in Oceanography 149, 134–144.

Shearman, D.J., Smith, A.J., 1985, Ikaite, the parent mineral of jarrowite-type pseudomorphs. Proceedings of the Geologists' Association 96, 305–314.

Shibuya, M., 1977, A study on the Gen'no-ishi: its mode of occurrence, form, and texture. The Journal of the Geological Society of Japan 83, 19–26.

Shikama, T., Kase, T., 1976, Molluscan fauna of the Miocene Morozaki Group in the southern part of Chita Peninsula, Aichi Prefecture, Japan. Science Reports of the Yokohama National University. Section 2, Biology and Geology 23, 1–25.

Soetaert, K., Hofmann, A.F., Middelburg, J.J., Meysman, F.J.R., Greenwood, J., 2007, The effect of biogeochemical processes on pH. Marine Chemistry 105, 30–51.

Spielhagen, R.F., Tripati, A., 2009, Evidence from Svalbard for near-freezing temperatures and climate oscillations in the Arctic during the Paleocene and Eocene. Palaeogeography, Palaeoclimatology, Palaeoecology 278, 48–56.

Stakes, D.S., Orange, D., Paduan, J.B., Salamy, K.A., Maher, N., 1999, Cold-seeps and authigenic carbonate formation in Monterey Bay, California. Marine Geology 159, 93–109.

Stein, C.L., Smith, A.J., 1986, Authigenic carbonate nodules in the Nankai Trough, Site 583. Initial Reports of the Deep Sea Drilling Project 87, 659–668.

Stockmann, G., Tollefsen, E., Skelton, A., Brüchert, V., Balic-Zunic, T., Langhof, J., Skogby, H., Karlsson, A., 2018, Control of a calcite inhibitor (phosphate) and temperature on ikaite precipitation in Ikka Fjord, southwest Greenland. Applied Geochemistry 89, 11–22.

Suess, E., Balzer, W., Hesse, K.F., Müller, P.J., Ungerer, C.A., Wefer, G., 1982, Calcium carbonate hexahydrate from organic-rich sediments of the Antarctic shelf: precursors of glendonites. Science 216, 1128–1131.

Suto, I., Yanagisawa, Y., Ogasawara, K., 2005, Tertiary geology and chronostratigraphy of the Joban area and its environs, northeastern Japan. Bulletin of the Geological Survey of Japan 56, 375–409.

Suzuki, A., 2000, An Eocene cold-water molluscan assemblage from the Poronai Formation in the Mikasa area, central Hokkaido, northern Japan. Earth Science 54, 363–368.

Takahashi, K., 1967, Hokoseki from the Magari-kawa River, Yamagata, Japan. Chigaku

Kenkyu 18, 185–188.*

Takano, O., Hoyanagi, K., Noto, M., Ota, K., Yahata, M., Sedimentary facies group of the Kabato Collaborative Research Group, 1996, Formation processes of depositional sequences of the Neogene System in the southern part of the Kabato Mountains, Hokkaido, Japan. Earth Science 50, 9–28.

Teichert, B.M.A., Luppold, F.W., 2013, Glendonites from an Early Jurassic methane seep—Climate or methane indicators? Palaeogeography, Palaeoclimatology, Palaeoecology 390, 81–93.

The Kabato Collaborative Research Group, 1995, Neogene stratigraphy of the Aoyama area, Tobetsu Town in the southern part of the Kabato Mountains, Hokkaido, Japan. Earth Science 49, 363–378.

Tollefsen, E., Balic-Zunic, T., Mörth, C.-M., Brüchert, V., Lee, C.C., Skelton, A., 2020, Ikaite nucleation at 35°C challenges the use of glendonite as a paleotemperature indicator. Scientific Reports 10, 8141.

Tollefsen, E., Stockmann, G., Skelton, A., Mörth, C.-M., Dupraz, C., Sturkell, E., 2018, Chemical controls on ikaite formation. Mineralogical Magazine 82, 1119–1129.

Tsushima, K., Kakimi, T., Ueda, T., 1956, Geology of the Atsuta district. Quadrangle Series, 1:50,000. Geological Survey of Japan.

Ueda, Y., Ando, H., Shinozaki, M., 2003, Depositional facies and their paleogeographic implications of the Oligocene Iwaki to Asagai formations, Shiramizu Group in northern Ibaraki Prefecture. Bulletin of Ibaraki Natural Museum 6, 1–17.

Vasileva, K., Vereshchagin, O., Ershova, V., Rogov, M., Chernyshova, I., Vishnevskaya, I., Okuneva, T., Pokrovsky, B., Tuchkova, M., Saphronova, N., Kostrov, Y., Khmarin, E., 2021, Marine diagenesis of ikaite: Implications from the

isotopic and geochemical composition of glendonites and host concretions (Palaeogene–Neogene sediments, Sakhalin Island). Sedimentology 68, 2227–2251.

Vickers, M., Watkinson, M., Price, G.D., Jerrett, R., 2018, An improved model for the ikaite-glendonite transformation: Evidence from the lower cretaceous of Spitsbergen, Svalbard. Norwegian Journal of Geology 98, 1–15.

Vickers, M.L., Lengger, S.K., Bernasconi, S.M., Thibault, N., Schultz, B.P., Fernandez, A., Ullmann, C. V, Mccormack, P., Bjerrum, C.J., Rasmussen, J.A., Hougård, I.W., Korte, C., 2020, Cold spells in the Nordic Seas during the early Eocene Greenhouse. Nature Communications 11, 4713.

Wang, Z., Wang, J., Suess, E., Wang, G., Chen, C., Xiao, S., 2017, Silicified glendonites in the Ediacaran Doushantuo Formation (South China) and their potential paleoclimatic implications. Geology 45, 115–118.

Whiticar, M.J., 1999, Carbon and hydrogen isotope systematics of bacterial formation and oxidation of methane. Chemical Geology 161, 291–314.

Yoshida, H., Asahara, Y., Yamamoto, K., Katsuta, N., Minami, M., Metcalfe, R., 2019, $^{87}Sr/^{86}Sr$ age determination by rapidly formed spherical carbonate concretions. Scientific Reports 9, 1003.

Yoshida, H., Ujihara, A., Minami, M., Asahara, Y., Katsuta, N., Yamamoto, K., Sirono, S., Maruyama, I., Nishimoto, S., Metcalfe, R., 2015, Early post-mortem formation of carbonate concretions around tusk-shells over week-month timescales. Scientific Reports 5, 14123.

Yoshida, H., Yamamoto, K., Minami, M., Katsuta, N., Sirono, S., Metcalfe, R., 2018, Generalized conditions of spherical carbonate concretion formation around decaying organic matter in early diagenesis. Scientific Reports 8, 6308.

Yoshida, H., Yamamoto, K., Ohe, T., Katsuta, N., Muramiya, Y., Metcalfe, R., 2020, Diffusion controlled formation of spherical carbonate concretion in muddy sedimentary matrices. Geochemical Journal 54, 233–242.

Zachos, J., Pagani, M., Sloan, L., Thomas, E., Billups, K., 2001, Trends, rhythms, and aberrations in global climate 65 Ma to present. Science 292, 686–693.

Zhou, X., Lu, Z., Rickaby, R.E.M., Domack, E.W., Wellner, J.S., Kennedy, H.A., 2015, Ikaite abundance controlled by porewater phosphorus level: Potential links to dust and productivity. The Journal of Geology 123, 269–281.

*English translation from the original written in Japanese

Figures and Tables

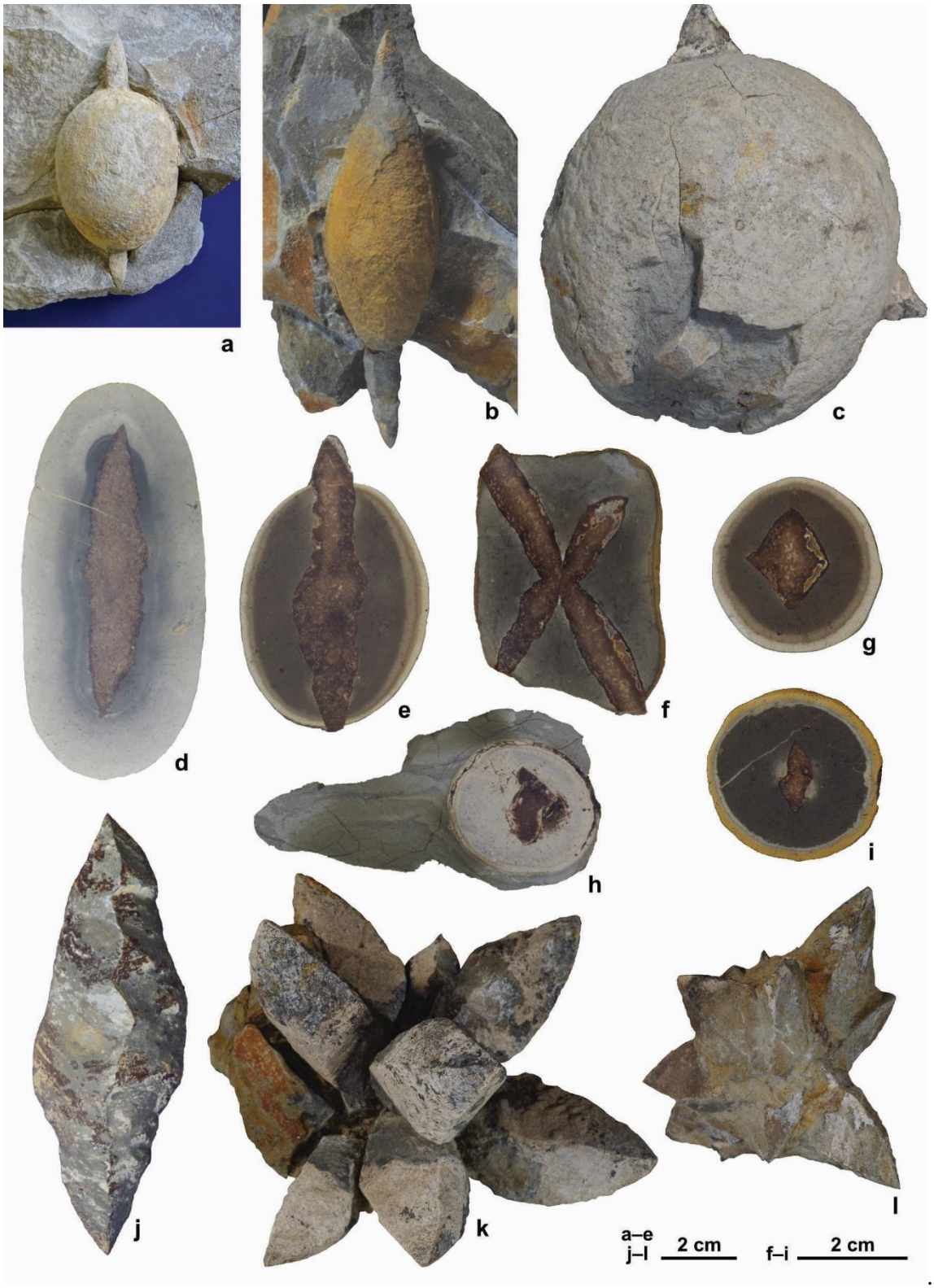

Figure 1. Various occurrences of glendonites and glendonite concretions. (a, b) Glendonite concretions with surrounding mudstone. Bipyramidal-shaped glendonites are contained in the center of concretions. The glendonite terminations thrust out a surface of concretions. (c) Glendonite concretion contains stellate-shaped glendonite in the center. The glendonite terminations thrust out a surface of concretions. (d) Vertical section of glendonite concretion. The concretion entirely envelops the glendonite. (e) Vertical section of glendonite concretion. The glendonite terminations thrust out a surface of concretions. (f) Glendonite concretion contains X-shaped glendonite. (g–i) Cross-sections of glendonite concretions. The relative size of the glendonites to the surrounding concretions varies from specimen to specimen. Laminae of the surrounding matrix bend around the concretion (h). (j) Bipyramidal-shaped glendonite without concretion. (k, l) Stellate-shaped glendonites without concretions. Specimen (h) is from the Toyohama Formation. Specimen (c), (k), and (l) are from the Asagai Formation. The other specimens are from the Poronai Formation. (After Muramiya and Yoshida (submitted)).

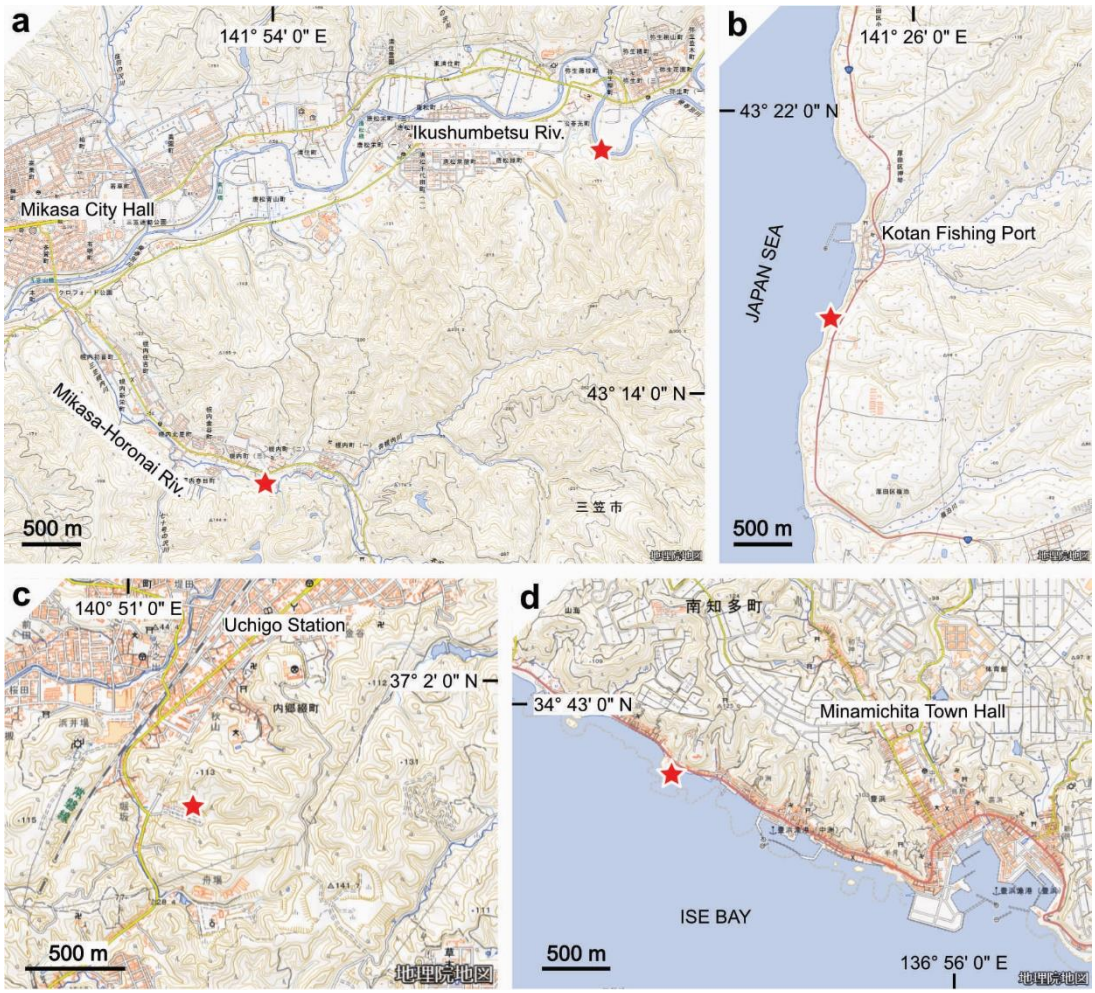

Figure 2. The exact localities of the studied glendonites. Red stars indicate the outcrop yielding glendonites. (a) Mikasa area where the Poronai Formation is distributed. (b) Ishikari area where the Morai Formation is distributed. (c) Iwaki area where the Asagai Formation is distributed. (d) Minamichita area where the Toyohama Formation is distributed. (After Muramiya et al., 2022)

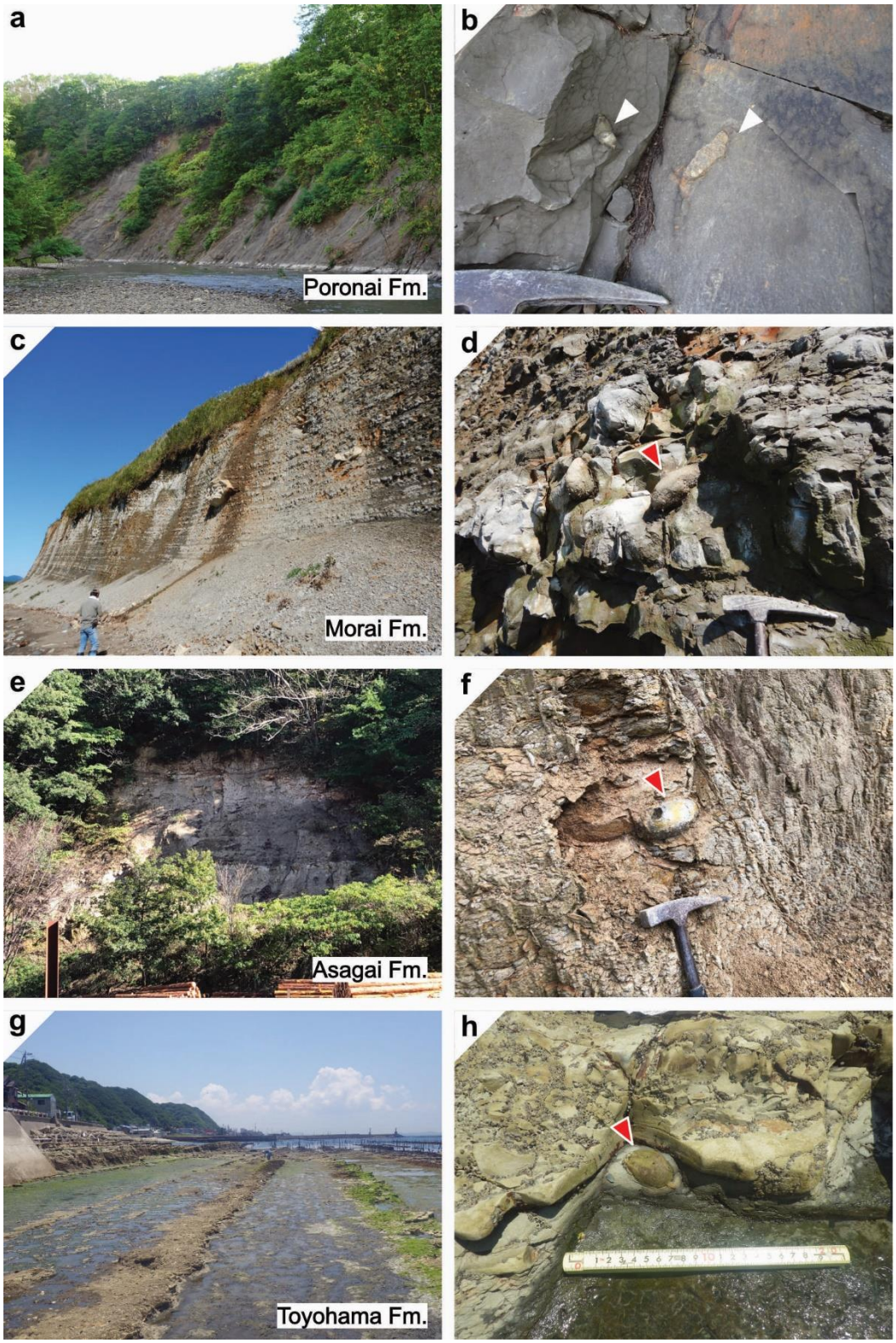
a
Poronai Fm.
b
c
Morai Fm.
d
e
Asagai Fm.
f
g
Toyohama Fm.
h

Figure 3. The glendonite-bearing strata and occurrences of glendonites. (a, b) The Poronai Formation crops out along the Ikushumbetsu River in Mikasa. Glendonites without concretions are contained in bioturbated dark-gray mudstone. (c, d) The Morai Formation crops out along the coast of the Japan Sea. Glendonite concretions contained weakly bedded light-gray mudstone. (e, f) The Asagai Formation crops out at the timber yard at Iwaki. Glendonite concretions are contained in bioturbated gray siltstone. (g, h) The Toyohama Formation crops out along the coast of Ise Bay. Glendonite concretions are contained in bioturbated dark-gray mudstone. (After Muramiya et al., 2022)

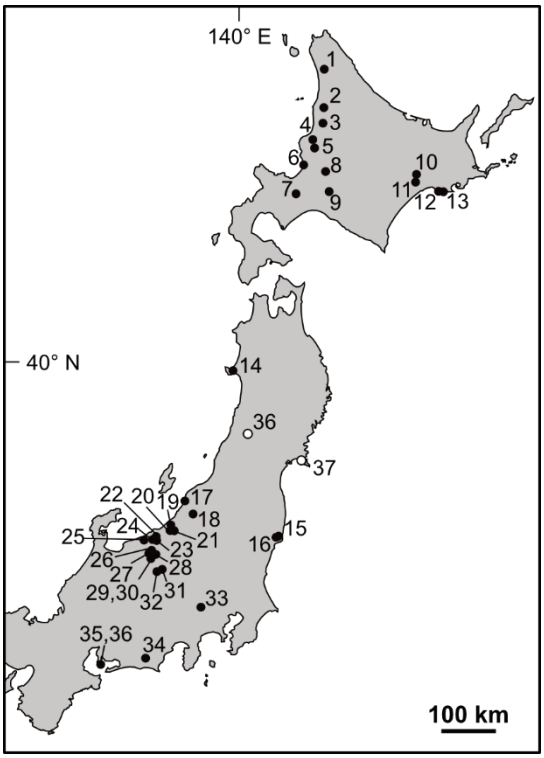

Figure 4. The localities of glendonites and Hokoseki in Japan. Numbers 1 to 35 (filled circles) indicate the localities of glendonites, and 36 and 37 (open circles) indicate the localities of Hokoseki. Table 1 shows the detail of each locality (After Muramiya and Yoshida (submitted)).

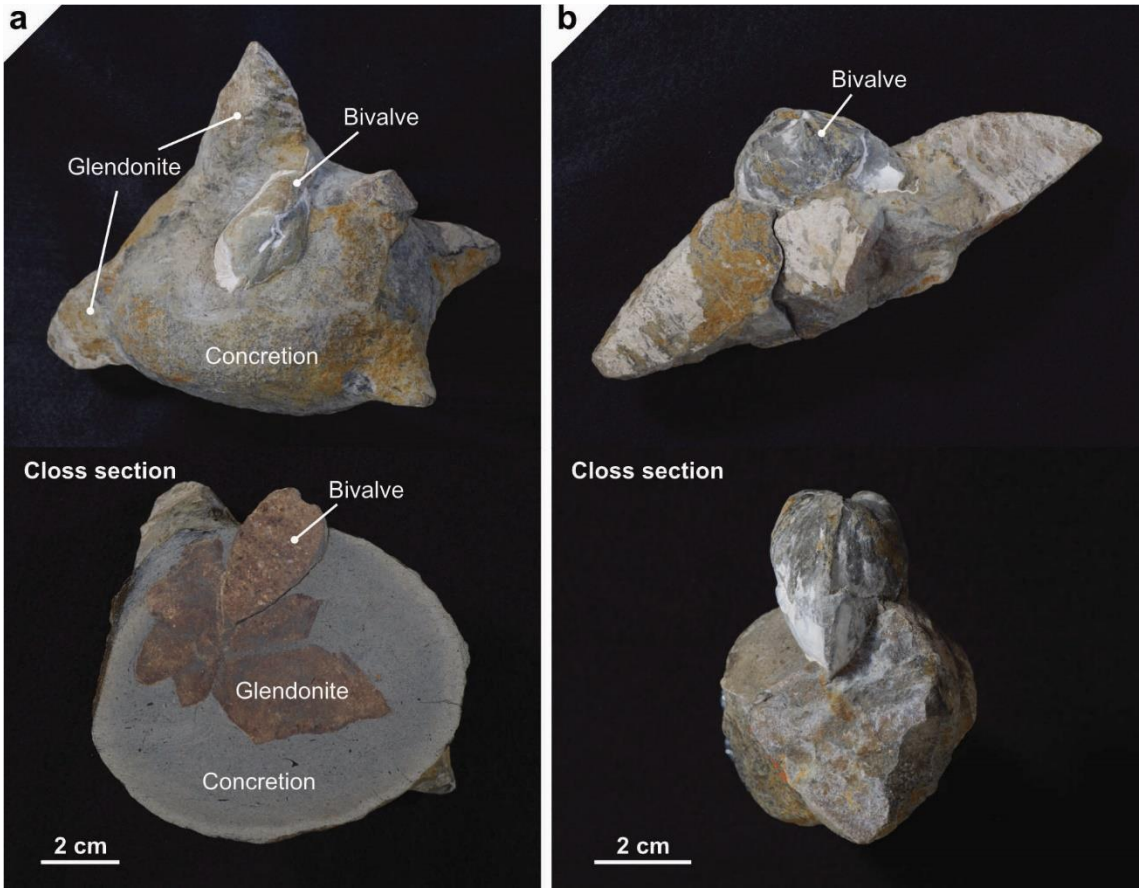

Figure 5. Glendonite (a) with and (b) without concretion formed around the ventral side of the articulated bivalve (*Mya grewingki*). Specimens are obtained from the Asagai Formation. (Modified from Muramiya and Yoshida (submitted))

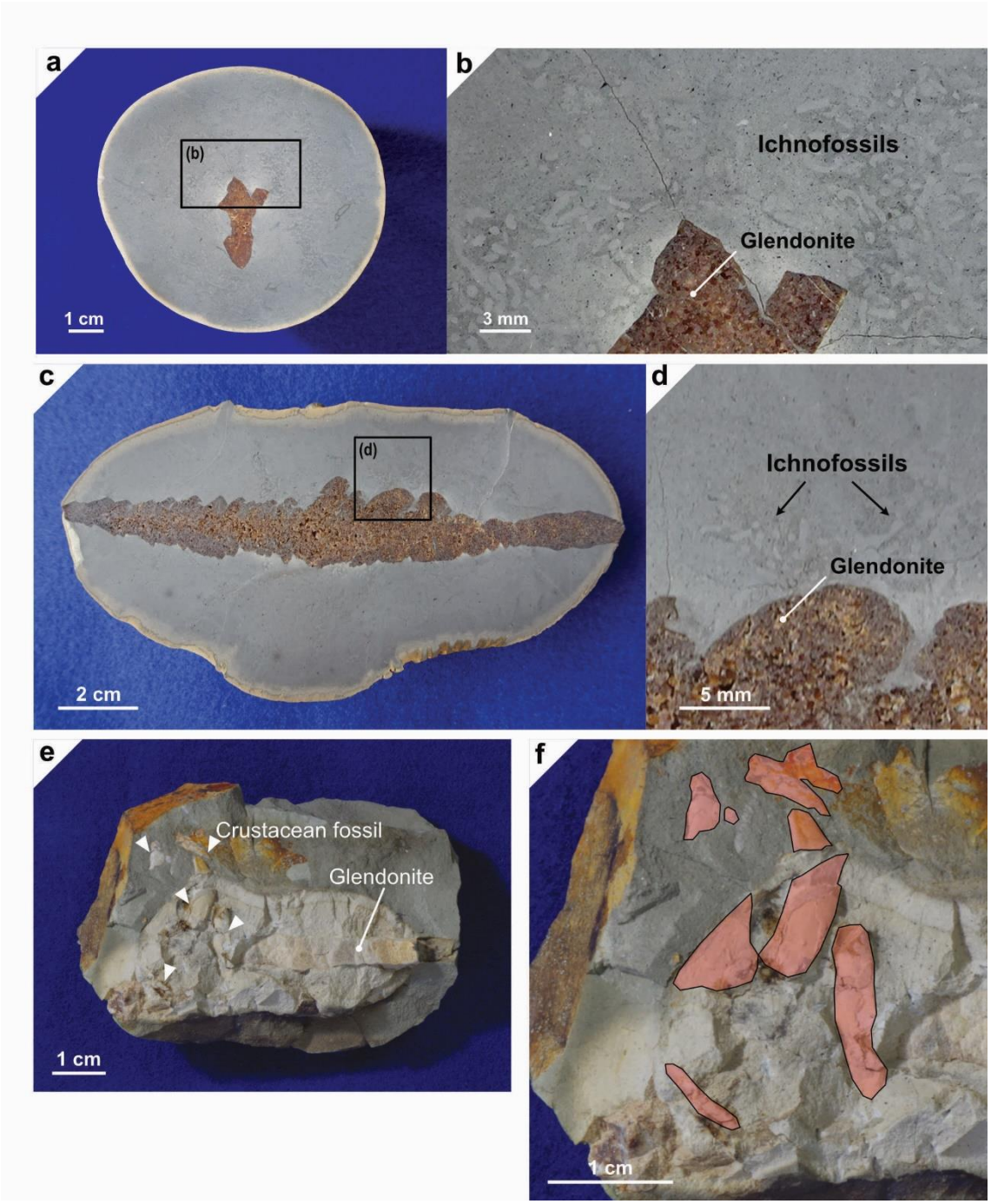

Figure 6. (a–d) Glendonite concretions containing an aggregation of small ichnofossils, and (e, f) glendonite concretion containing crustacean fossils. (f) The red shaded areas indicate crustacean fossils. Specimens (a) and (d) are obtained from the Morai Formation, and specimen (e) is from the Toyohama Formation.

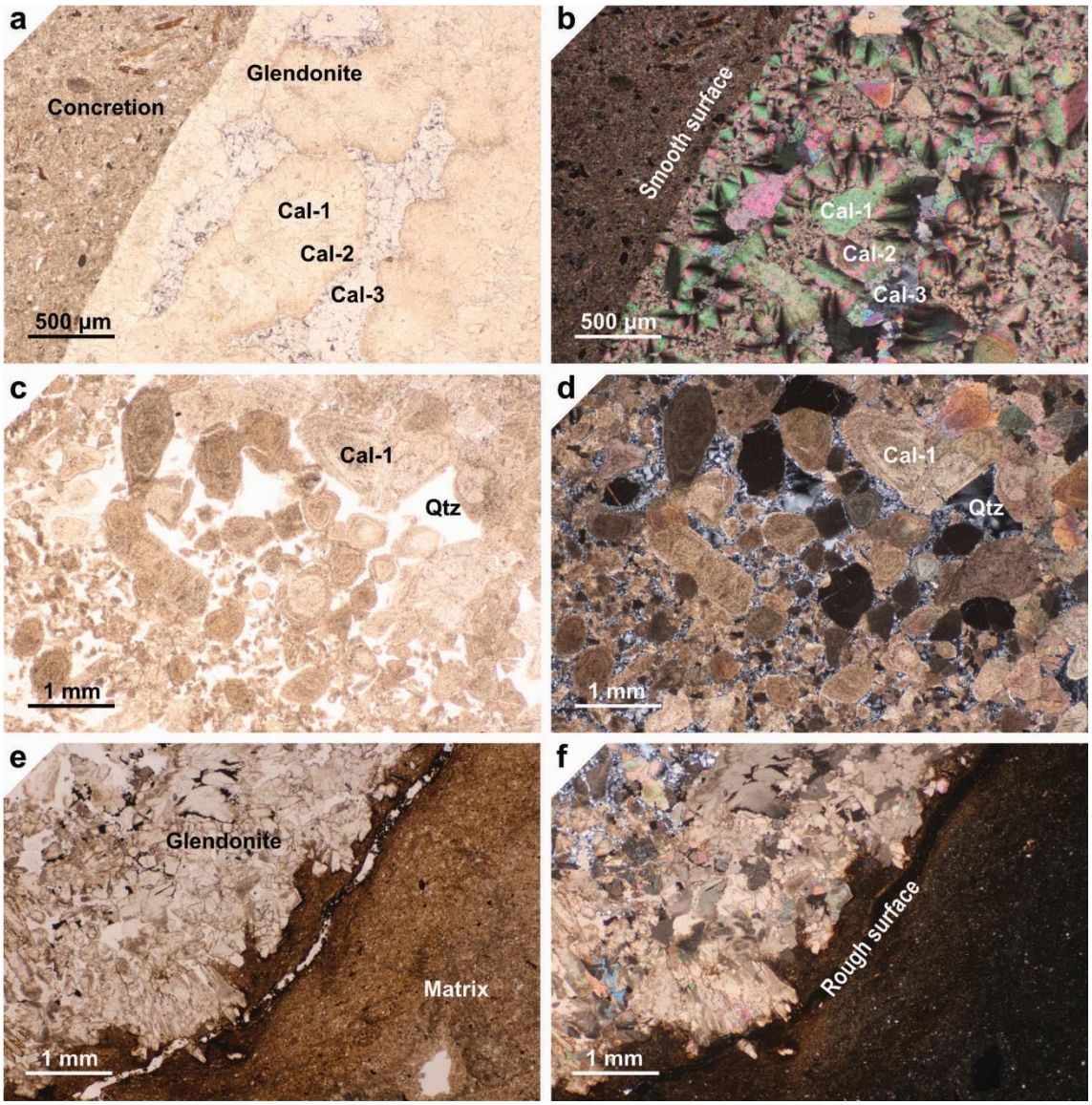

Figure 7. Thin-section microphotographs of glendonites from the Poronai Formations. (a, b) Photomicrographs of glendonite concretion. Glendonite in concretion comprises three types of calcites: elliptical or polygonal-shaped granular calcite derived from ikaite (Cal-1), radiaxial calcite formed around cal-1 (Cal-2), and sparitic calcite filling remaining pores (Cal-3). The surface of glendonite is smooth. (c–f) Photomicrographs of glendonite without concretion, comprising granular calcite (Cal-1) and pore-filling quartz (Qtz). The surface of glendonite is rough.

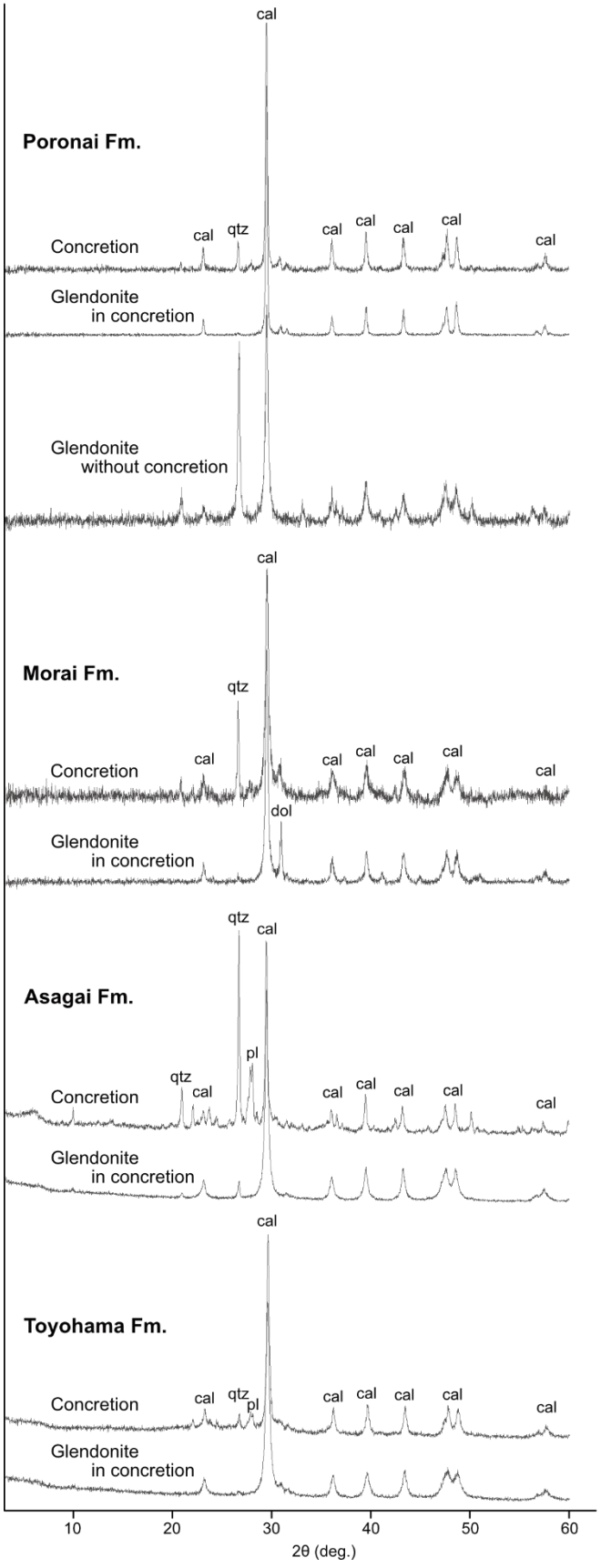
Poronai Fm.
Concretion
Glendonite
in concretion
Glendonite
without concretion
cal
qtz
Morai Fm.
dol
Asagai Fm.
pl
Toyohama Fm.
10
20
30
40
50
60
2θ (deg.)

Figure 8. Mineral compositions of glendonites and surrounding concretions determined using XRD analyses. Concretions around glendonites comprise calcite (cal) and minor amounts of quartz (qtz) and plagioclase (pl). Glendonites in concretions comprise calcite and a minor amount of dolomite (dol). Glendonite without concretion is composed of calcite and quartz.

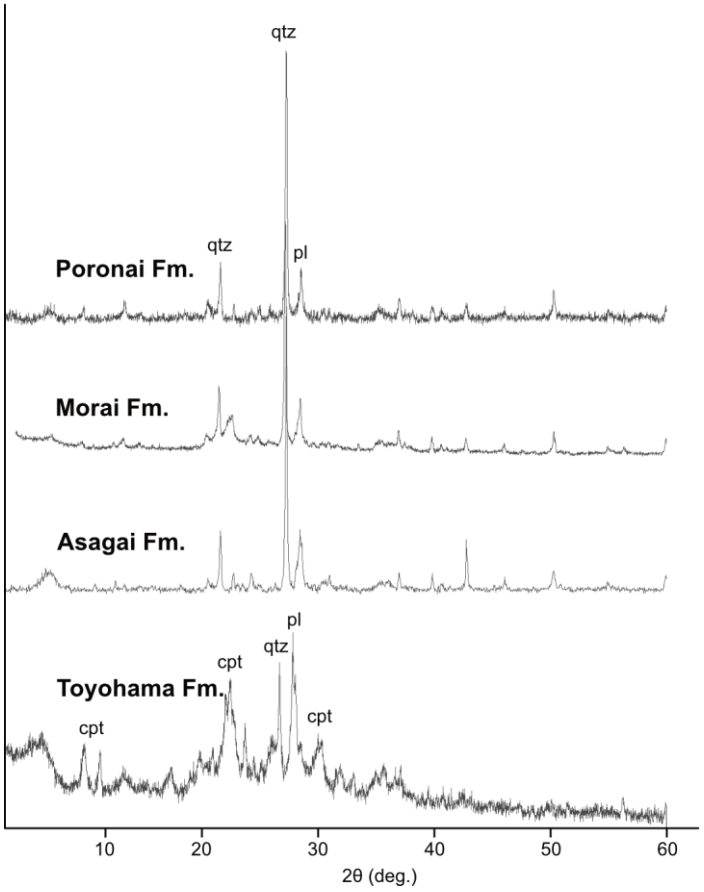

Figure 9. Mineral compositions of surrounding matrixes determined using XRD analyses. Matrixes of the Poronai, Morai, and Asagai formations comprise quarts (qtz) and plagioclase (pl). The matrix of the Toyohama Formation contains clinoptilolite (cpt), quartz, and plagioclase.

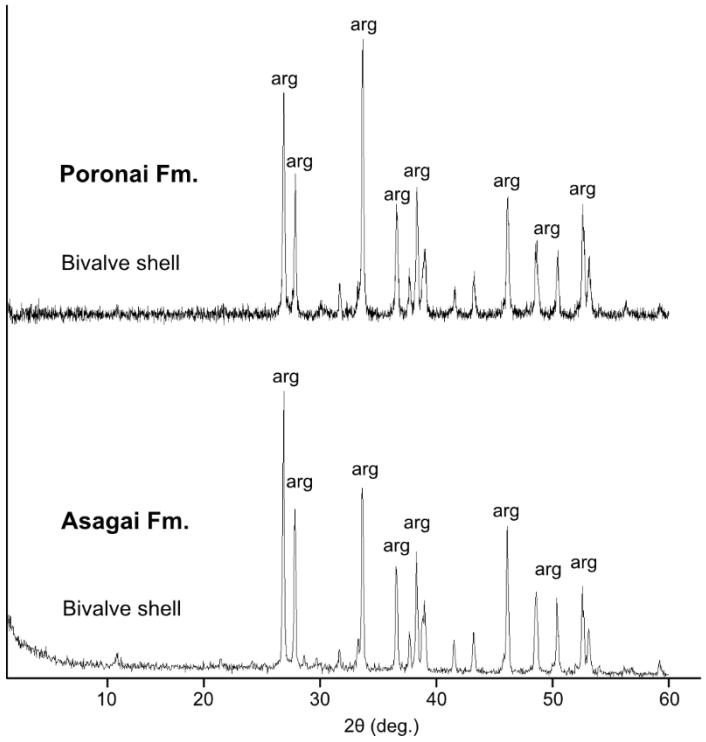

Figure 10. Mineral compositions of bivalve shells from the Poronai and Asagai formations determined using XRD analyses. Bivalve shells comprise aragonite (arg).

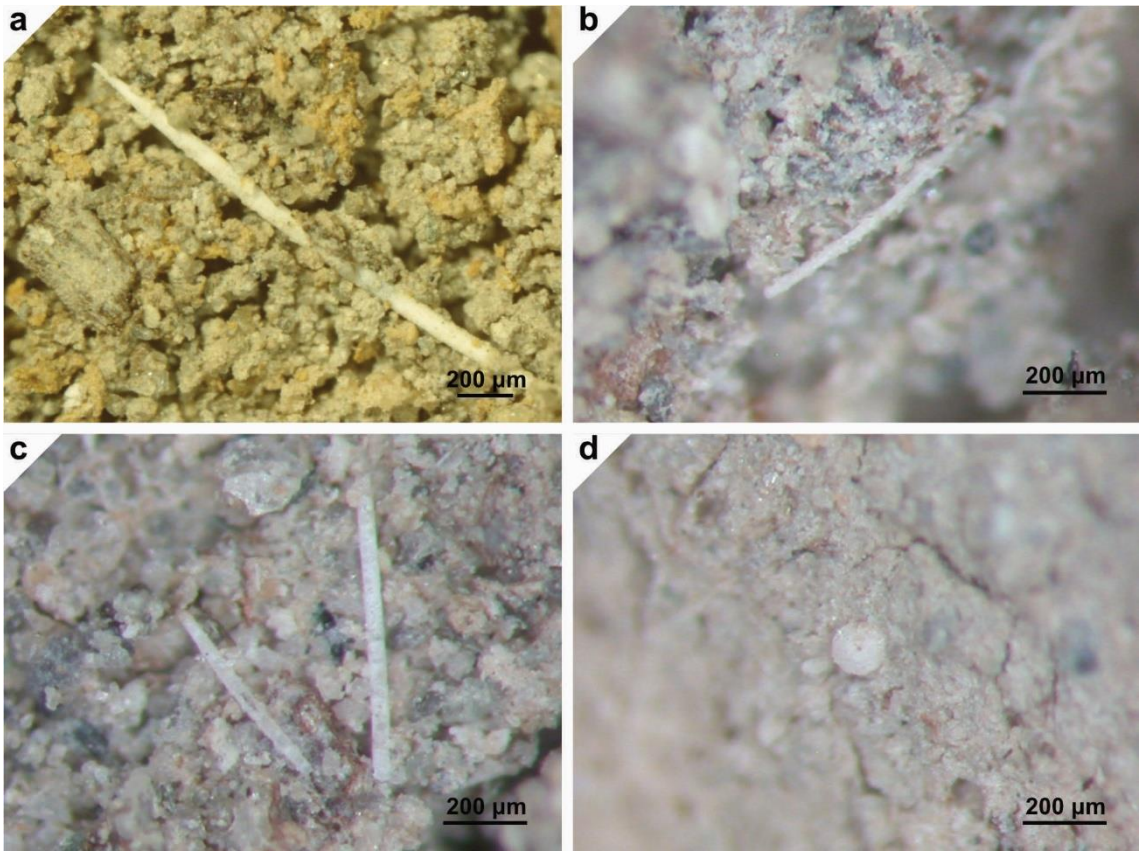

Figure 11. Small shelly fossils extracted from concretions around glendonites of the Poronai Formations. (a–c) Needle-shaped fossils—sclerites of sponges. (d) Disk-shaped fossils—shells of foraminifera.

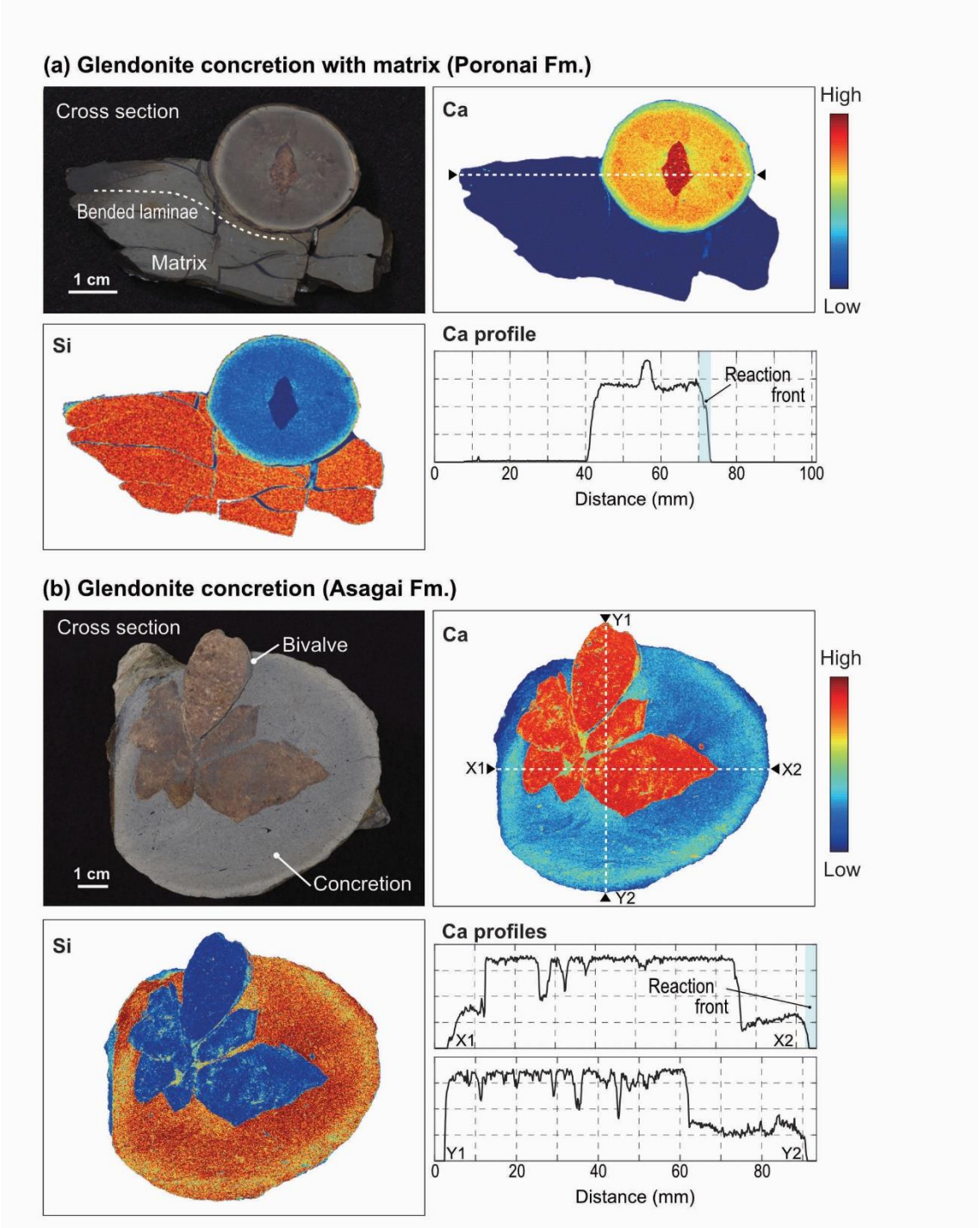

Figure 12. Elemental distributions in and around glendonite concretions. (a) Glendonite concretion with surrounding mudstone from the Poronai Formation. (b) Glendonite concretion containing bivalve from the Asagai Formation. Ca distributes homogeneously

in concretion and decreases steeply at a concretion margin (reaction front). Ca is hardly detected in surrounding mudstone. Si shows an inverse distribution to Ca. (After Muramiya et al., 2022)

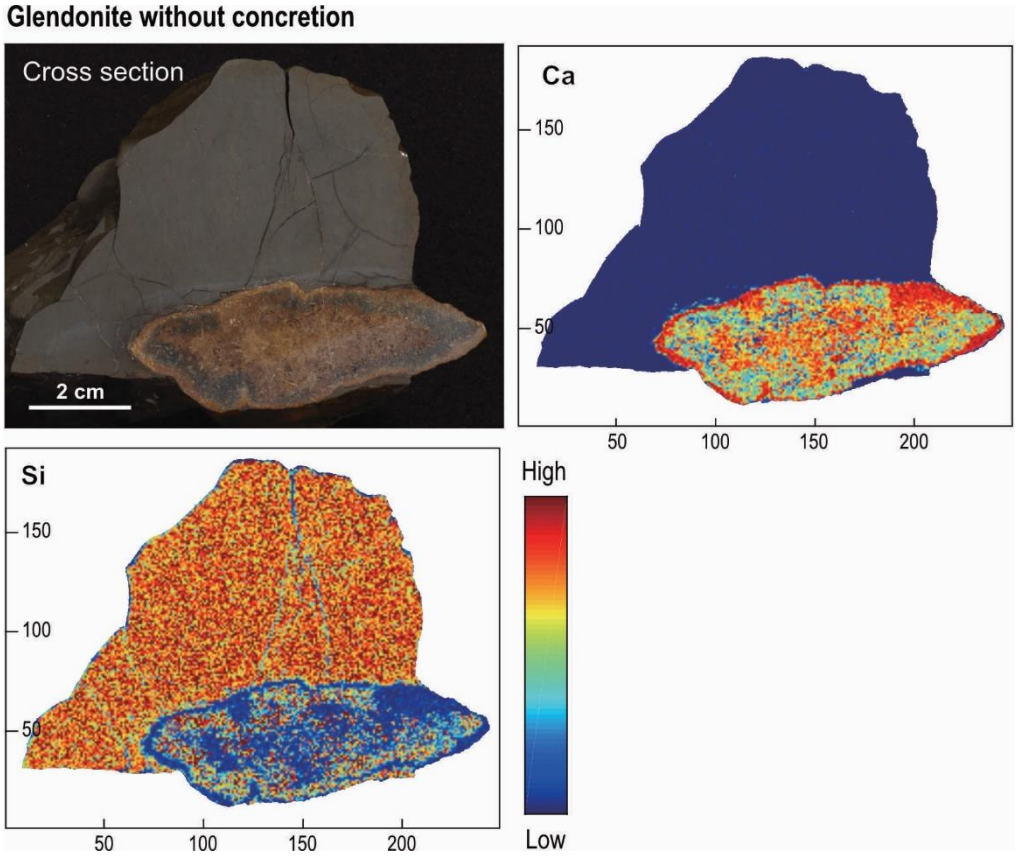

Figure 13. Elemental distributions in and around glendonite. Ca and Si are concentrated in glendonite, and Ca is hardly detected in surrounding mudstone. The sample for analysis was obtained from the Poronai Formation.

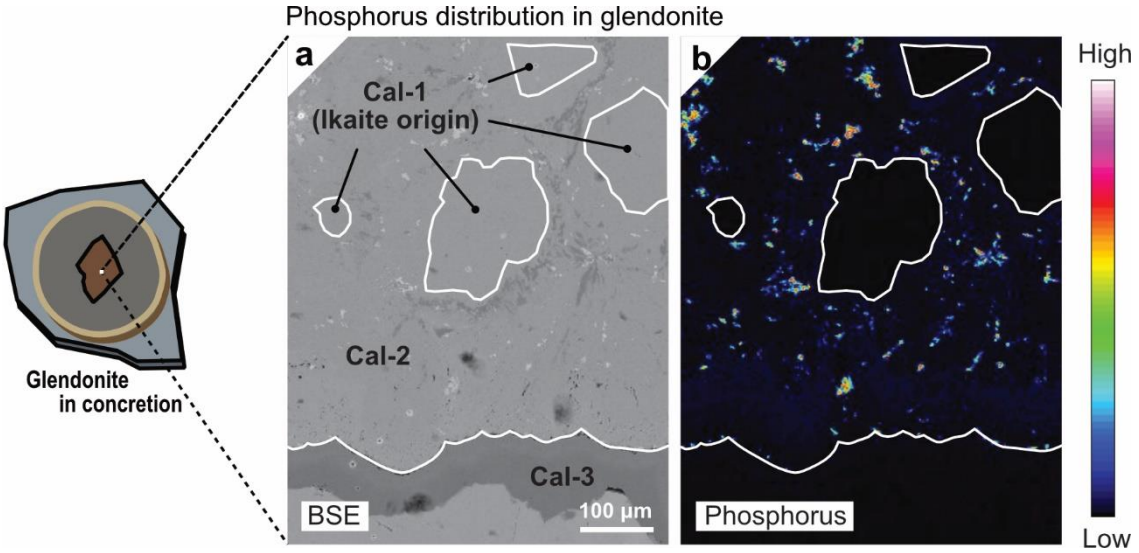

Figure 14. Phosphorus distribution in glendonite. (a) Backscattered electron image. (b) Phosphorus distribution. Phosphorus concentrates in Cal-2. (After Muramiya and Yoshida (submitted))

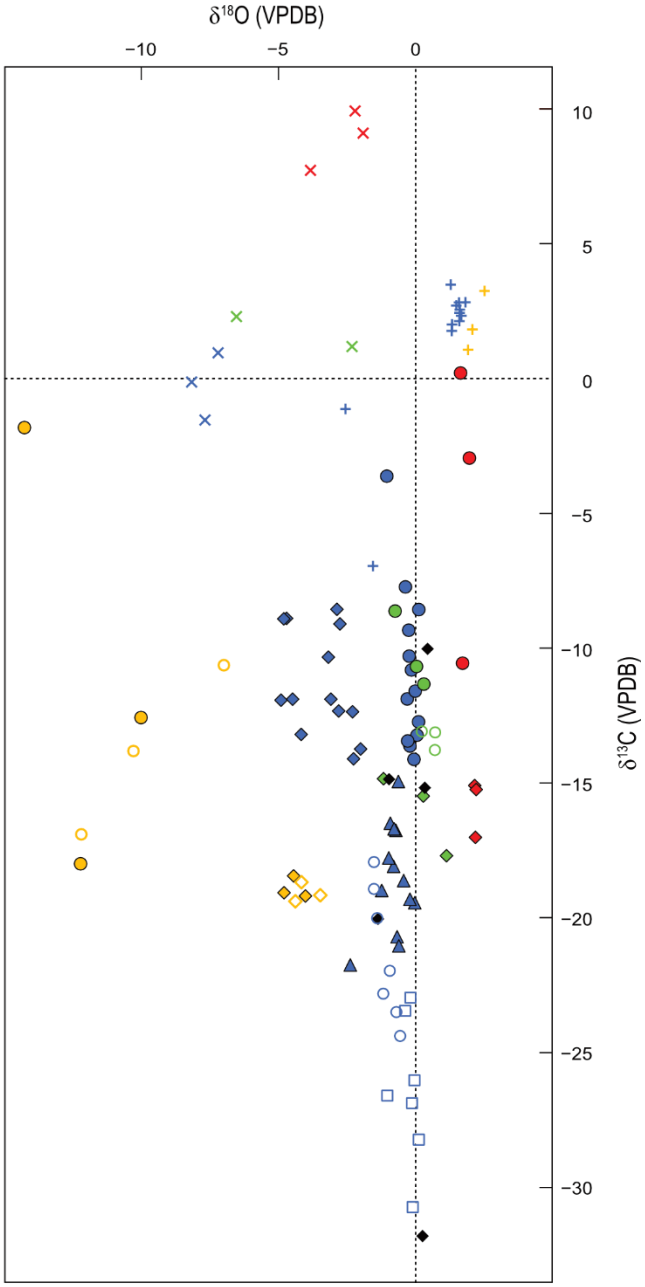

	Poronai Fm.	Morai Fm.	Asagai Fm.	Toyohama Fm.
Glendonite in concretions (bulk)	◆	◆	◆	◆
Glendonite in concretions (in bivalve, bulk)			◇	
Cal-1	▲			
Concretion around glendonite	●	●	●	●
Concretion around glendonite (in bivalve)			○	
Glendonite without concretions (bulk)	◆			
Concretion around ghost shrimp	○			○
Concretion around bivalve	□			
Bivalve shell	+		+	
Carbonates in mudstone	×	×		×

Figure 15. Stable oxygen and carbon isotopic compositions ($\delta^{18}O$ and $\delta^{13}C$). Data is shown in Table 4.

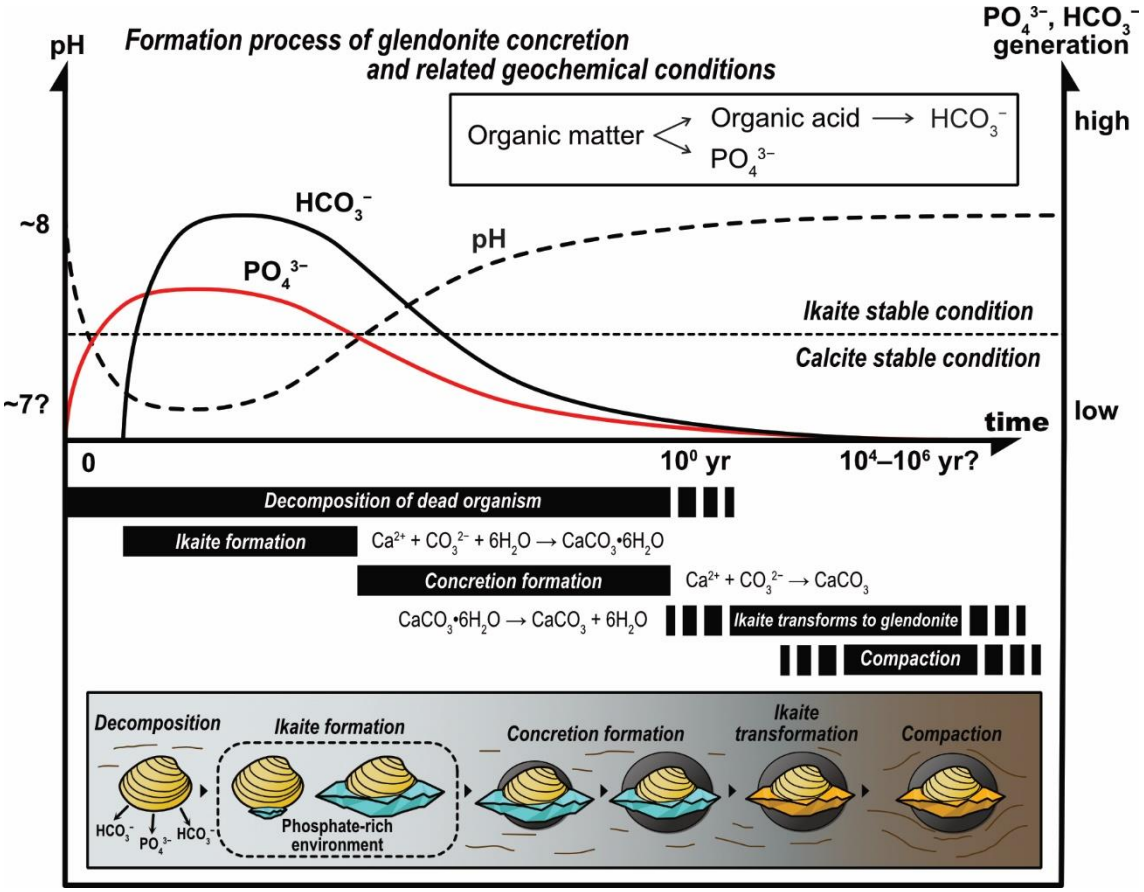

Figure 16. The schematic formation process of glendonite concretion and related geochemical conditions. In a phosphate-rich environment, ikaite crystals form using bicarbonate derived from organic decomposition. When phosphate concentrations fall below the ikaite stability threshold, the growth of ikaite crystals ceases, and calcite concretions begin to form. The concretion growth continues until all carbon is consumed. The phosphorus concentration is presumably controlled by porewater pH, determined by the balance between organic acid generation by organic decomposition and buffering by seawater. (Modified from Muramiya et al., 2022)

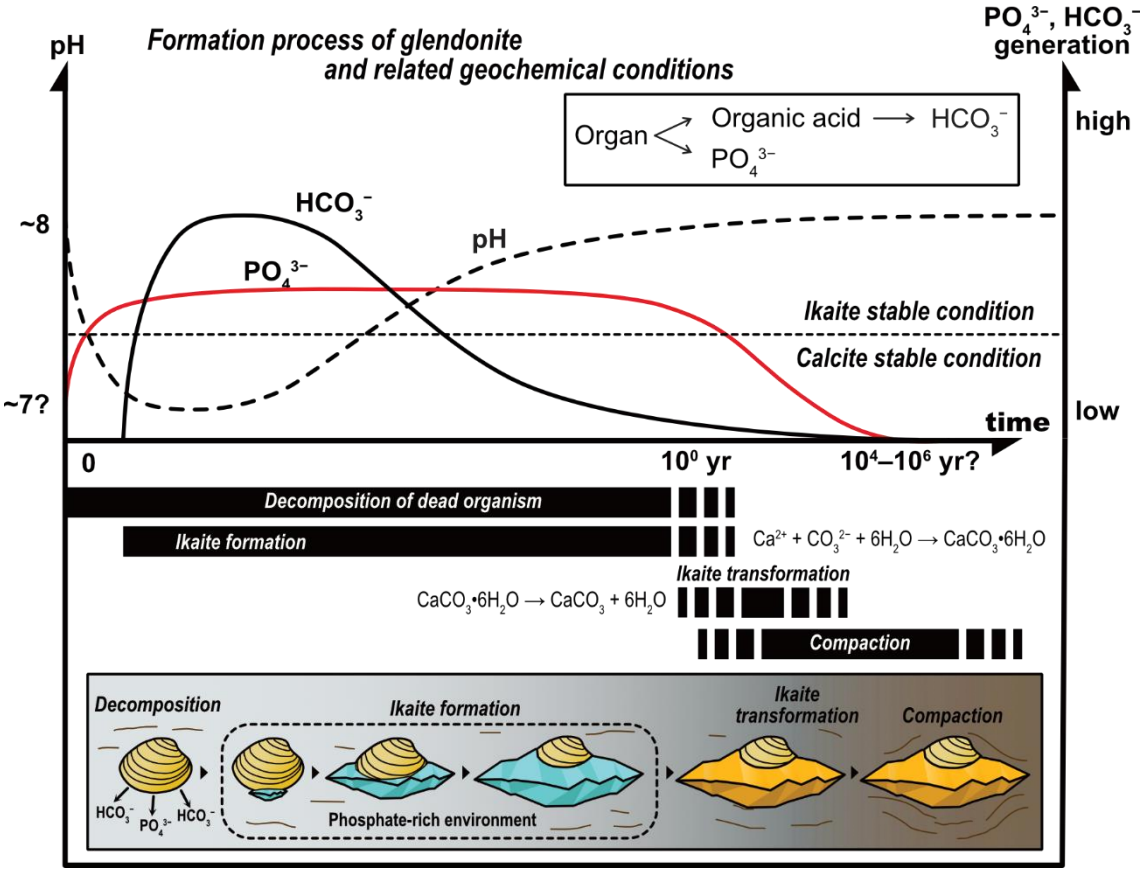

Figure 17. The schematic formation process of glendonite and related geochemical conditions. In a phosphate-rich environment, ikaite crystals form using bicarbonate derived from organic decomposition. When phosphate concentration is kept higher than the threshold of ikaite stabilization throughout the decomposition, all bicarbonate derived from a dead organism is used for ikaite crystal growth.

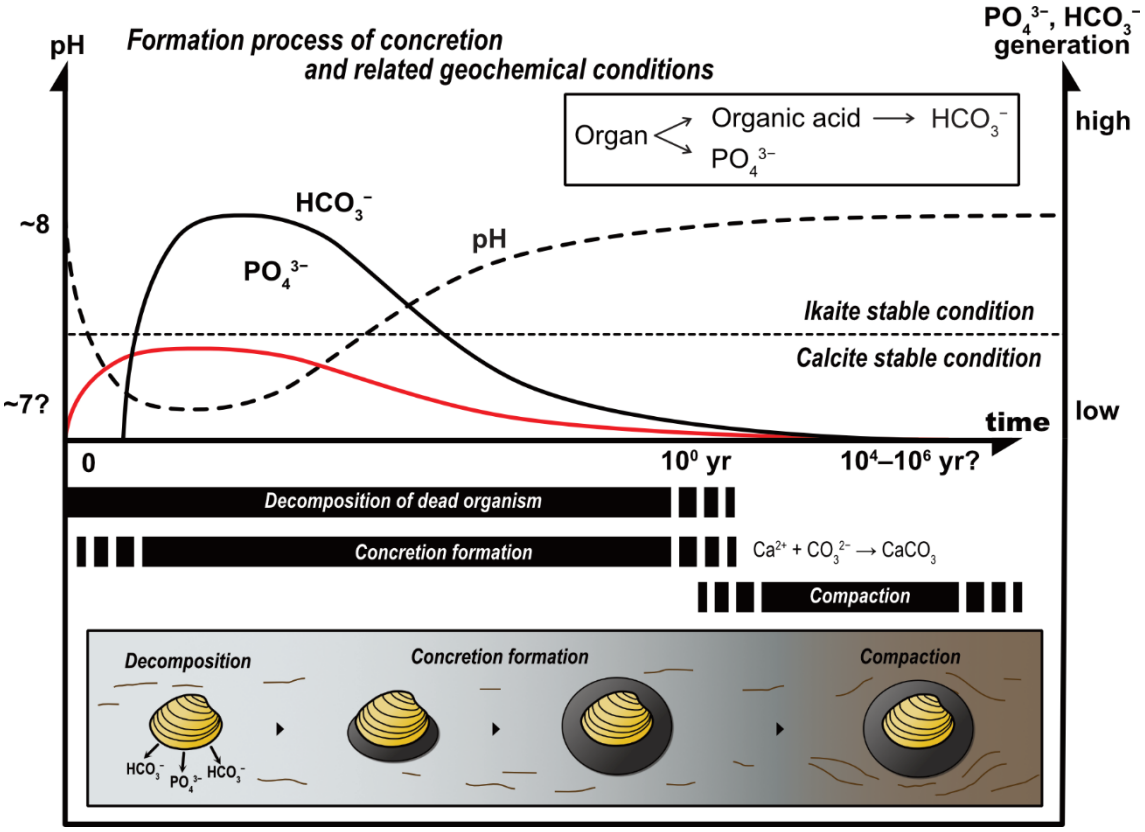

Figure 18. The schematic formation process of concretion and related geochemical conditions. When phosphate concentration is kept lower than the threshold of ikaite stabilization and/or temperature is too high for ikaite precipitation, all bicarbonate derived from a dead organism is used for calcite concretion formation.

Table 1. The distributions, ages, facies, and paleobathymetric depths of glendonite-bearing formations in Japan. The references are shown in Muramiya and Yoshida (2020). (Modified from Muramiya and Yoshida, 2020)

Name of formations	Distributions	Depositional age	Facies	Paleobathymetric depth	Glendonite without concretion	Glendonite concretion
1 Yuchi Fm.	Northern Hokkaido	Pliocene	Unbedded sandy siltstone.	Sublittoral	●	●
2 Sankebetsu Fm.	Northern Hokkaido	Late Eocene	Silty fine sandstone. Abundant fossils of marine mollusks and concretions containing shell fossils or glendonites.	Outer shelf, inner to outer sublittral		●
3 Tappu Fm.	Northern Hokkaido	Late Eocene	Massive dark-gray mudstone. Concretions containing shell fossils, crustacean fossils, or glendonites.	Upper bathyal		●
4 Mashike Fm.	Central Hokkaido	Late Miocene	Dark-gray to gray mudstone.			●
5 Toppu Fm.	Central Hokkaido	Late Miocene	Soft and gray mudstone. Concretions containing glendonites.	Sublittoral to bathyal		●
6 Morai Fm.	Central Hokkaido	Late Miocene	Bedded silicic mudstone.	200–300 m		●
7 Ichinosawa Fm. (Misumai Shale Mem.)	Central Hokkaido	Miocene	Dark-gray mudstone with intercalations of thin tuffaceous sandstone. Concretions.			●
8 Poronai Fm.	Central Hokkaido	Late Eocene	Massive dark-gray mudstone. Concretions containing shell fossils, crustacean fossils, or glendonites.	Lower sublittoral to upper bathyal	●	●
9 Momijiyama Chukan Fm.	Central Hokkaido	Eearly Oligocene	Dark-gray mudstone. Concretions containing shell fossils or glendonites.	Outer sublittoral to littoral		●
10 Omagari Fm.	Eastern Hokkaido	Late Eocene	Blue-gray fine sandstone. Fossils of shell and brittle star.	Sublittoral		
11 Charo Fm.	Eastern Hokkaido	Eearly Oligocene	Dark-gray to black mudstone.Concretions containing shell fossils or glendonites.	Upper bathyal		●
12 Shitakara Fm.	Eastern Hokkaido	Late Eocene	Light yellowish gray sandy mudstone to muddy fine sandstone. Abundant fossils of marine organisms.	Sublittoral	●	●
13 Soun Fm.	Eastern Hokkaido	Late Eocene to early Oligocene*	Light-gray to dark-gray mudstone.	Estuarine	●	●

Table 1. (continued)

Name of formations	Distributions	Depositional age	Facies	Paleobathymetric depth	Glendonite without concretion	Glendonite concretion
14 Wakimoto Fm.	northern Akita	Middle Pleistocene	Sandy mudstone, muddy sandostone, and sandostone. Concretions cantaining glendonites	Several hundreds meters		●
15 Shirasaka Fm.	Southern Fukushima	Early Oligocene	Massive blue-gray mudstone.	Upper shoreface to inner shelf	●	●
16 Asagai Fm.	Southern Fukushima	Early Oligocene	Gray to greenish-gray sandstone. Glendonites are contained in muddy part.	Outer shelf to upper slope shelf	●	●
17 Teradomari Fm.	Central Niigata	Middle to late Miocene	Alternating beds of greenish-gray mudstone and grayish-white sandstone. Glendonites are contained in muddy part.	Bathyal to abyssal	●	
18 Araya Fm.	Central Niigata	Late Miocene	Massove dark-gray to blackish-gray mudstone. Concretions.			●
19 Ogaya Fm.	Central Niigata	Middle to late Miocene	Weakly bedded bluish-graymudstone with intercalations of thin tuff.	1000–2000 m		
20 Tamugigawa Fm.	Central Niigata	Pliocene	Alternating beds of sandstone and mudstone with thick sandstone, sandy siltsone, and mudstone.	150–250 m		
21 Shobu Fm.	Central Niigata	Pliocene	Massive dark-gray mudstone.	150–250 m		
22 Noya Fm. (Yokohata Mem.)	Southern Niigata	Late Miocene	Alternating beds of sandstone and mudstone, massive dark-gray mudstone. Glendonites are contained in mudstone or shale.	1000–2000 m		
23 Nambayama Fm.	Southern Niigata	Middle to late Miocene	Alternating beds of sandstone and mudstone. Glendonites are contained in mudstone.	2000 m	●	
24 Hiuchiyama Fm.	Southern Niigata	Middle to late Miocene	Bedded hard black shale.			
25 Nechi Fm.	Southern Niigata	Late Miocene to early Pliocene	Bioturbated massive gray sandy mudstone and muddy sandstone. Concretions.	Lower sublittoral to upper bathyal		
26 Tanogashira Fm.	Northern Nagano	Early Pliocene	Almost massive mudstone and sandy mudstone with intercalation of alternating beds of sandstone and mudstone.		●	

Table 1. (continued)

Name of formations	Distributions	Depositional age	Facies	Paleobathymetric depth	Glendonite without concretion	Glendonite concretion
27 Kinasa Fm. (Rihei Conglomerate-Mudstone Mem.)	Northen Nagano	Late Miocene to Pliocene	Massive dark-gray to black mudstone with intercalation of sandstone, conglomerate, and tuff.			
28 Asagawa Mudstone Fm.	Northen Nagano	Middle Miocene	Light-gray to dark-gray mudstone.		●	
29 Machi Sandy Mudstone Fm.	Northen Nagano	Late Miocene to Pliocene	Dark-black to dark-gray mudstone with intercalation of alternation beds of sandostone and mudstone. Glendonites are contained in muddy part.			
30 Ronchi Mudstone Fm.	Northen Nagano	Miocene	Gray to dark-gray fine to midium sandstone.			
32 Bessho Fm.	Central Nagano	Middle Miocene	Blackish-gray mudstone.	Littoral to upper bathyal	●	
31 Iseyama Fm.	Central Nagano	Middle Miocene	Bedded black shale.			
33 Kosho Alternatiom Mem.	Western Tokyo	Middle Miocene	Alternation beds of massive blackish-gray mudstone and calcareous fine sandstone. Glendonites are contained in both facies.	>200 m	●	●
34 Towata Fm.	Western Shizuoka	Early Miocene	Massive dark-gray siltstone.		●	●
35 Toyohama Fm.	Southern Aichi	Early Miocene	Alternation beds of dark-gray mudstone and gray tuff. Glendonites are contained in mudstone. Concretions containing crustacean fossils and glendonites.	Batyal		●

Table 2. Quantitative elemental composition data determined using XRF analyses. Phosphorus concentrates in glendonites in concretions and the surrounding concretions compared with matrixes. (After Muramiya et al., 2022)

Formation	Sample name	Sample type	SiO_2	TiO_2	Al_2O_3	Fe_2O_3	MnO	MgO	CaO	Na_2O	K_2O	P_2O_5	LOI	Total
Poronai	Pb01	Concretion around glendonite	13.5	0.2	3.2	1.8	0.1	1.3	41.4	0.4	0.4	1.6	34.3	98.2
Poronai	Pc01	Concretion around glendonite	15.0	0.2	3.7	1.9	0.1	1.9	39.8	0.5	0.5	0.8	33.9	98.2
Poronai	Pc04	Concretion around glendonite	29.8	0.1	2.7	1.5	0.0	1.5	28.8	0.2	0.2	0.6	34.9	100.4
Poronai	Pc06	Concretion around glendonite	13.6	0.2	3.3	1.7	0.1	2.3	41.3	0.4	0.3	0.9	35.3	99.1
Poronai	Pc12	Concretion around glendonite	23.5	0.1	2.4	1.4	0.0	1.9	32.7	0.3	0.2	0.7	36.1	99.5
Poronai	Pc17	Concretion around glendonite	26.5	0.2	3.4	1.8	0.0	1.8	31.4	0.4	0.4	0.7	33.3	99.7
Poronai	Pb01	Glendonite in concretion (bulk)	2.3	0.0	0.6	0.8	0.0	1.7	51.4	0.1	0.0	1.2	43.1	101.3
Poronai	Pc01	Glendonite in concretion (bulk)	2.2	0.0	0.1	0.8	0.0	1.6	51.5	0.1	0.0	1.0	43.1	100.5
Poronai	Pc04	Glendonite in concretion (bulk)	1.4	0.0	0.3	0.9	0.0	1.9	53.2	0.1	0.0	1.1	42.8	101.7
Poronai	Pc06	Glendonite in concretion (bulk)	1.1	0.1	0.3	1.1	0.0	1.6	54.0	0.1	0.0	1.0	42.9	102.1
Poronai	Pc12	Glendonite in concretion (bulk)	1.7	0.0	0.2	0.9	0.0	1.8	51.3	0.1	0.0	1.0	44.4	101.5
Poronai	Pc17	Glendonite in concretion (bulk)	1.4	0.1	0.3	1.1	0.0	1.8	53.1	0.1	0.0	1.1	43.0	101.9
Poronai	Pa01	Glendonite without concretion (bulk)	16.7	0.0	0.2	3.1	0.0	0.9	43.4	0.1	0.0	0.1	34.2	98.8
Poronai	Pc02	Glendonite without concretion (bulk)	11.3	0.1	0.5	1.5	0.1	0.5	47.9	0.2	0.1	0.1	39.5	101.7
Poronai	Pa03	Glendonite without concretion (bulk)	12.9	0.1	0.3	1.4	0.1	0.5	47.9	0.1	0.0	0.1	38.7	102.1
Poronai	Pa04	Glendonite without concretion (bulk)	16.6	0.0	0.2	2.9	0.1	2.5	42.4	0.1	0.0	0.1	34.9	99.8
Poronai	Pa05	Glendonite without concretion (bulk)	13.7	0.1	0.6	2.9	0.1	0.6	45.5	0.1	0.1	0.1	36.1	99.7
Poronai	Po-mtrx01	Matrix	67.2	0.7	14.6	5.6	0.0	2.1	0.9	1.8	2.7	0.1	5.1	100.7
Poronai	Po-mtrx02	Matrix	65.0	0.7	13.8	5.9	0.0	2.1	1.3	1.7	2.5	0.1	6.0	98.9
Poronai	Po-mtrx03	Matrix	65.1	0.6	13.4	4.9	0.0	1.7	1.6	2.1	2.4	0.1	5.4	97.5
Poronai	Po-mtrx04	Matrix	65.3	0.7	13.5	5.2	0.0	1.9	1.4	1.7	2.4	0.1	5.5	97.7
Poronai	Po-mtrx05	Matrix	63.2	0.7	14.8	5.4	0.0	2.0	1.0	1.9	2.6	0.1	5.3	97.1
Morai	Ko01	Concretion around glendonite	16.2	0.2	3.6	1.8	0.1	3.8	37.4	0.5	0.5	0.8	33.9	98.9
Morai	Ko05	Concretion around glendonite	15.3	0.2	3.5	1.7	0.1	4.4	36.8	0.5	0.5	0.6	35.2	98.8
Morai	Ko06	Concretion around glendonite	17.4	0.2	3.8	1.9	0.1	4.0	35.4	0.6	0.5	0.7	34.0	98.6
Morai	Ko01	Glendonite in concretion (bulk)	2.2	0.0	0.2	0.7	0.0	2.7	50.7	0.1	0.0	0.9	43.7	101.1
Morai	Ko05	Glendonite in concretion (bulk)	1.5	0.0	0.1	1.2	0.0	3.0	51.7	0.1	0.0	0.8	43.5	102.2
Morai	Ko06	Glendonite in concretion (bulk)	1.6	0.0	0.1	0.9	0.0	2.8	51.7	0.1	0.0	0.8	44.1	102.3
Morai	Ko-mtrx01	Matrix	62.9	0.6	12.3	5.0	0.0	2.5	0.9	1.9	2.2	0.1	9.5	97.8
Morai	Ko-mtrx02	Matrix	64.2	0.6	13.0	4.8	0.0	2.6	1.2	1.9	2.2	0.1	9.3	99.9
Morai	Ko-mtrx03	Matrix	63.8	0.6	12.7	4.7	0.0	2.7	1.2	1.8	2.2	0.1	9.7	99.5
Asagai	Iw01g	Concretion around glendonite	46.3	0.4	10.8	3.2	0.2	1.0	17.6	1.8	1.7	0.6	16.5	100.1
Asagai	Iw02g	Concretion around glendonite	42.4	0.4	9.6	2.8	0.2	0.9	21.4	1.6	1.5	0.4	19.1	100.3
Asagai	Iw03g	Concretion around glendonite	24.7	0.3	6.6	2.3	0.9	0.7	33.5	1.0	0.9	0.5	27.7	99.1
Asagai	Iw01g	Concretion around glendonite (in bivalve)	37.3	0.3	8.2	2.8	0.2	0.7	25.0	1.4	1.3	0.4	22.0	99.6
Asagai	Iw02g	Concretion around glendonite (in bivalve)	29.4	0.3	6.4	1.8	0.2	0.6	31.9	1.1	1.0	0.5	26.5	99.5
Asagai	Iw03g	Concretion around glendonite (in bivalve)	24.6	0.2	5.6	2.0	0.2	0.7	34.2	1.0	0.9	0.8	28.1	98.2
Asagai	Iw01g	Glendonite in concretion (bulk)	5.2	0.1	0.6	0.9	0.2	0.4	52.9	0.2	0.1	0.2	41.8	102.5
Asagai	Iw02g	Glendonite in concretion (bulk)	4.9	0.1	0.8	1.0	0.2	0.4	52.6	0.2	0.1	0.2	41.8	102.4
Asagai	Iw03g	Glendonite in concretion (bulk)	4.6	0.1	0.5	1.1	0.2	0.4	52.9	0.1	0.0	0.2	42.1	102.3
Asagai	Iw01g	Glendonite in concretion (in bivalve, bulk)	2.1	0.1	0.2	0.8	0.2	0.5	54.7	0.1	0.0	0.2	43.5	102.3
Asagai	Iw02g	Glendonite in concretion (in bivalve, bulk)	2.9	0.1	0.3	0.9	0.2	0.4	54.1	0.1	0.0	0.2	43.4	102.5
Asagai	Iw03g	Glendonite in concretion (in bivalve, bulk)	2.5	0.1	0.2	1.1	0.2	0.4	54.5	0.1	0.0	0.2	43.4	102.8
Asagai	Iw-mtrx01	Matrix	64.8	0.6	15.1	3.2	0.0	1.3	2.5	2.4	2.4	0.1	6.5	98.9
Asagai	Iw-mtrx02	Matrix	65.4	0.6	15.8	3.3	0.0	1.2	2.5	2.6	2.3	0.1	6.1	100.0
Asagai	Iw-mtrx03	Matrix	63.3	0.5	15.9	3.7	0.0	1.4	2.4	2.3	2.2	0.1	8.1	100.0
Toyohama	Mo01g	Concretion around glendonite	23.7	0.3	5.7	2.7	0.2	2.8	31.8	1.2	0.8	0.9	29.1	99.0
Toyohama	Mo02g	Concretion around glendonite	28.2	0.3	6.3	2.8	0.3	2.0	28.1	1.5	1.0	0.9	27.4	98.8
Toyohama	Mo03g	Concretion around glendonite	21.5	0.3	5.1	2.6	0.3	2.0	32.8	1.0	0.7	0.9	31.0	98.3
Toyohama	Mo04g	Concretion around glendonite	16.4	0.3	4.3	2.6	0.3	2.3	36.6	0.7	0.5	1.1	33.1	98.2
Toyohama	Mo01	Glendonite in concretion (bulk)	2.7	0.1	0.5	0.9	0.1	2.7	50.7	0.2	0.0	1.0	42.9	101.9
Toyohama	Mo02g	Glendonite in concretion (bulk)	4.3	0.0	0.3	0.8	0.0	2.5	47.2	0.1	0.0	1.1	42.4	98.8
Toyohama	Mo03g	Glendonite in concretion (bulk)	1.8	0.1	0.2	1.0	0.0	3.1	51.6	0.1	0.0	1.1	43.1	102.1
Toyohama	Mo04g	Glendonite in concretion (bulk)	1.8	0.1	0.1	1.2	0.0	2.7	52.1	0.1	0.0	1.1	43.1	102.4
Toyohama	Mo-mtrx01	Matrix	55.2	0.8	13.5	5.3	0.0	1.7	2.2	2.7	2.5	0.1	13.8	97.9
Toyohama	Mo-mtrx02	Matrix	56.7	0.6	12.5	4.6	0.0	1.5	1.6	3.0	2.5	0.1	15.4	98.5
Toyohama	Mo-mtrx03	Matrix	56.6	0.7	13.0	4.8	0.0	1.5	2.1	2.7	2.6	0.1	13.7	97.9

Table 3. Elemental compositions in high phosphorus concentration area in glendonite. Data are expressed as cation ratio in %. (After Muramiya et al., 2022)

No.	Mg	P	K	Al	S	Ca	Si	Fe	Mn	Total
1	0.659	27.772	0.000	0.051	0.062	71.418	0.000	0.038	0.000	100
2	0.684	30.104	0.001	0.103	0.000	69.000	0.000	0.108	0.000	100
3	0.967	19.500	0.000	0.022	0.048	79.434	0.000	0.030	0.000	100
4	0.388	22.103	0.000	0.000	0.079	77.384	0.000	0.032	0.013	100

Table 3. $\delta^{13}C$ and $\delta^{18}O$ values of glendonite concretions and related samples. Data in Fig. 15 are shown here. (After Muramiya et al., 2022)

		Sample type					
		Concretion around glendonite		Glendonite in concretion (bulk)		Cal-1	
Formation	Sample name	$\delta^{13}C$ (‰VPDB)	$\delta^{18}O$ (‰VPDB)	$\delta^{13}C$ (‰VPDB)	$\delta^{18}O$ (‰VPDB)	$\delta^{13}C$ (‰VPDB)	$\delta^{18}O$ (‰VPDB)
Poronai	Pc01	-10.8	-0.2	-11.9	-3.1	-19.4	0.0
Poronai	Pc04	-8.6	0.1	-8.6	-2.9	-20.7	-0.7
Poronai	Pc06	-12.7	0.1	-12.3	-2.8	-21.8	-2.4
Poronai	Pc07	-11.9	-0.3	-10.3	-3.2	-16.8	-0.7
Poronai	Pc09	-13.6	-0.2	-13.2	-4.2	-19.3	-0.2
Poronai	Pc10	-3.6	-1.1	-9.1	-2.8	-14.9	-0.6
Poronai	Pc12	-13.2	0.1	-14.1	-2.3	-21.0	-0.6
Poronai	Pc13	-9.3	-0.3	-8.9	-4.7	-16.5	-0.9
Poronai	Pc17	-11.6	0.0	-12.4	-2.3	-16.7	-0.8
Poronai	Pc20	-13.4	-0.3	-11.9	-4.5	-18.1	-0.8
Poronai	Pc22	-10.3	-0.2	-8.9	-4.8	-17.8	-1.0
Poronai	Pc23	-7.7	-0.4	-11.9	-4.9	-19.0	-1.2
Poronai	Pc24	-14.1	-0.1	-13.7	-2.0	-18.6	-0.4
Morai	Ko01	-10.6	1.7	-15.1	2.2		
Morai	Ko02	0.2	1.6	-15.2	2.2		
Morai	Ko03	-2.9	2.0	-17.0	2.2		
Asagai	Iw01	-18.0	-12.2	-19.1	-4.8		
Asagai	Iw01(in bivalve)	-16.9	-12.2	-19.2	-3.5		
Asagai	Iw02	-12.6	-10.0	-19.2	-4.0		
Asagai	Iw02(in bivalve)	-13.8	-10.3	-19.4	-4.4		
Asagai	Iw03	-1.8	-14.3	-18.4	-4.4		
Asagai	Iw03(in bivalve)	-10.6	-7.0	-18.7	-4.2		
Toyohama	Mo02	-8.6	-0.8	-14.8	-1.2		
Toyohama	Mo03	-10.7	0.0	-15.5	0.3		
Toyohama	Mo04	-11.3	0.3	-17.7	1.1		

Table 4. (continued)

Formation	Sample name	Glendonite without concretion (bulk) $\delta^{13}C$ (‰VPDB)	$\delta^{18}O$ (‰VPDB)
Poronai	Pa03	-20.0	-1.4
Poronai	Pa04	-15.2	0.3
Poronai	Pa05	-31.8	0.2
Poronai	Pa06	-14.9	-1.0
Poronai	Pa07	-10.0	0.4
		Concretion around fossil	
Poronai	Pd15 (Crustacea)	-17.9	-1.5
Poronai	Pd16 (Crustacea)	-22.0	-0.9
Poronai	Pd17 (Crustacea)	-22.8	-1.2
Poronai	Pd18 (Crustacea)	-20.0	-1.4
Poronai	Pd19 (Crustacea)	-18.9	-1.5
Poronai	Pd20 (Crustacea)	-24.4	-0.6
Poronai	Pd21 (Crustacea)	-23.5	-0.7
Poronai	Pc32 (bivalve)	-26.6	-1.0
Poronai	Pc33 (bivalve)	-30.7	-0.1
Poronai	Pc34 (bivalve)	-23.5	-0.4
Poronai	Pc35 (bivalve)	-26.0	0.0
Poronai	Pc36 (bivalve)	-28.2	0.1
Poronai	Pc37 (bivalve)	-26.9	-0.1
Poronai	Pc38 (bivalve)	-23.0	-0.2
Toyohama	Mo05 (Crustacea)	-13.1	0.7
Toyohama	Mo06 (Crustacea)	-13.1	0.2
Toyohama	Mo07 (Crustacea)	-13.8	0.7
		Bivalve shell fossil	
Poronai	18051401-1	2.1	1.6
Poronai	18051401-2	2.8	1.6
Poronai	18051401-3	2.7	1.5
Poronai	18051506-1	2.0	1.3
Poronai	18051506-2	2.3	1.7
Poronai	18051506-3	1.8	1.3
Poronai	18051502-1	3.5	1.3
Poronai	18051704-1	-7.0	-1.6
Poronai	18051704-2	-1.1	-2.6
Poronai	18051508-1	2.4	1.6
Poronai	18051508-2	2.6	1.6
Poronai	18051508-3	2.8	1.8
Asagai	Iw01shell	1.1	1.9
Asagai	Iw02shell	1.8	2.1
Asagai	Iw03shell	3.3	2.5
		Carbonates in matrix	
Poronai	Pc-mtrx01	1.0	-7.2
Poronai	Pc-mtrx02	-1.5	-7.7
Poronai	Pc-mtrx03	-0.1	-8.2
Morai	Ko-mtrx-01	7.7	-3.8
Morai	Ko-mtrx-02	9.1	-1.9
Morai	Ko-mtrx-03	9.9	-2.2
Toyohama	Mo-mtrx01	2.3	-6.5
Toyohama	Mo-mtrx02	-0.2	-2.3
Toyohama	Mo-mtrx03	1.2	-2.3

Table 5. Values for calculating the carbon content in the glendonite concretion. (After Muramiya et al., 2022)

Concretion		Cal-1	
x_{CaO} (%)	17.64	x_{CaO} (%)	54.00
ρ (g cm^{-3})	2.2	ρ (g cm^{-3})	2.7
V (cm^3)	207	V (cm^3)	65.1